Plasma Sources Sci. Technol. 1 (1992) 36–58. Printed in the UK

Measurements of electron energy distribution in low-pressure RF discharges

V A Godyak, R B Piejak and B M Alexandrovich
GTE Laboratories Incorporated, 40 Sylvan Road, Waltham, MA 02254, USA

Received 14 October 1991, in final form 18 November 1991

Abstract. Electron energy distribution functions (EEDFs) have been measured in low-pressure capacitive RF discharges over a wide range of well defined (geometrically and electrically) discharge conditions. Measurements have been made in argon and helium ranging in gas pressure between 3 mTorr and 3 Torr and in discharge current density between 0.1 mA cm^{-2} and 10 mA cm^{-2}. The measurements show changes in the EEDF due to the occurrence of physical phenomena such as stochastic electron heating and the effect of discharge transition into the γ mode. Substantial differences in the EEDF in Ramsauer and non-Ramsauer gases are also demonstrated and discussed. To achieve these results a higher level of performance was required from the measurement system than had been attained in previous EEDF measurements in RF discharges. EEDF measurements were made using a probe system specifically designed to remove or reduce the severity of many problems inherent to such measurements in RF discharges. The rationale and considerations in the probe system design, as well as many construction details of the probe system itself, are discussed.

1. Introduction

Widespread application of low-temperature plasma devices in modern technology has stimulated an extensive study of low-pressure capacitive (E-type) RF discharges. Typical RF discharges in such devices are characterized by the following parameters: driving frequency $\omega = 13.56$ MHz, gas pressure–electrode gap product pL between 10 mTorr cm and 10 Torr cm, driving voltage V_d between tens and hundreds of volts and discharge current density J between a fraction and tens of mA cm^{-2}. Under such conditions corresponding plasma parameters are: plasma density n between 10^8 and 10^{12} cm^{-3} and mean electron energy $\langle\varepsilon\rangle$ between 0.1 and 10 eV. In many instances, low-pressure RF discharge plasmas display a variety of non-equilibrium conditions. The electrons in such plasmas are not in local or temporal equilibrium with the space–time-variable RF field; they are also not in energetic equilibrium with ions and neutrals, nor are they in equilibrium within their own ensemble. Thus they manifest an essential departure from a Maxwellian distribution. Due to the extreme complexity of calculating the electron energy distribution function (EEDF), or $F(\varepsilon)$, in space–time variable self-consistent RF fields, Boltzmann equation treatments and particle simulation techniques require significant simplification (mainly by omission of essential processes of electron and atom interactions) and calculated EEDFs are but qualitative in nature. Therefore, experimental study of EEDFs in RF plasma is extremely important for understanding physical processes and calculating reaction rates, especially in complicated chemically reactive plasma where particle interaction diversity coupled with uncertainties in corresponding cross sections makes it extremely difficult to realistically calculate the EEDF.

Langmuir probe diagnostic methods are ideally suitable for plasma parameters encountered in low-pressure gas discharges. A modification of this method, known as the Druyvesteyn method [1], where the EEDF is inferred from the second derivative of the probe current/voltage characteristic, has been used for the last three decades to measure EEDFs in many different kinds of low-pressure discharge. An overview of different techniques for measuring EEDFs in gas discharge plasma is given in [2].

In the last decade, with increasing interest in the electron kinctics of plasma processing reactors, there have been many attempts to use probe measurements in such devices, resulting in surprising contradictions in plasma parameters obtained under apparently similar discharge conditions. It appears that the contradictions in the obtained results are a consequence of differences in probe measurement systems, the probes themselves, probe circuits, probe characteristic processing techniques and, in some cases, uncertainties in defining the RF discharge conditions. In this respect, the issue of the

0963-0252/92/010036+23 $04.50

proper design of probe experiments in RF discharge plasmas should be considered as no less (if not more) important than the results themselves.

In what follows, problems generally encountered in making EEDF measurements in low-pressure discharges will be discussed, emphasizing the special problems that must be faced when the measurements are made in RF excited discharges and the correct application of the Langmuir probes in RF discharge plasmas. The term 'low pressure' as referred to Langmuir probe applications implies a 'collisionless probe' regime (see section 2.1) corresponding to gas pressures lower than a few Torr. In section 3 an experimental system specifically designed for probe measurements in low-pressure RF discharges is described. The system is designed to remove or reduce the many problems inherent in EEDF measurements in low-pressure RF discharge and to provide continuous monitoring of the EEDF during RF discharge operation. In section 4, EEDF measurements made over a wide range of discharge conditions are presented along with a discussion of the different electron heating and ionization processes and related physical phenomena that correspond to the measured EEDFs. Improved overall probe system performance has been attained and, for the first time, the effect of stochastic electron heating and the effect of discharge transition into the γ mode on the EEDF in Ramsauer and non-Ramsauer gases are demonstrated.

2. EEDF measurement problems in RF discharges

The simplicity of the concept on which probe diagnostics are based has promoted the widespread illusion that measurement, processing and interpretation of probe characteristics are commonplace and routine. Indeed, 'There is no plasma diagnostic method other than probe diagnostics where the danger of incorrect measurements and erroneous interpretation of results is so great' [3]. In measuring the I/V characteristic of a probe, it is important to realize that even small errors, which are tolerable in classical Langmuir probe diagnostics, can result in enormous distortion in EEDFs found through differentiation of the probe's I/V characteristics, due to error magnification inherent in the differentiation procedure. Therefore, when an EEDF is obtained from the Druyvesteyn formula, special attention should be paid to the accuracy of the probe measurements themselves and to the correct application and limitations of traditional probe techniques. Note that the Druyvesteyn formula is only valid when the EEDF is essentially isotropic. Analysis of recent works on EEDF measurements in RF plasmas shows that the major problems in these works are related not only to the specific behaviour of probes in the RF plasma but also to the neglect of well established requirements and limitations for traditional probe methods, and to archaic probe measuring and differentiation techniques which were proved in the 1960s to be inadequate for EEDF measurement.

Overviews of modern EEDF measurement techniques and a discussion of the specific problems encountered in EEDF measurements in RF plasmas have been written by one of the present authors [2, 4]. So here, we will briefly comment on some issues that have not been properly addressed in recent publications on measuring the EEDF in RF discharges and which are important to understand the guidelines used in designing our experimental set-up. More details about these issues can be found in [2, 4] and in the literature cited therein.

2.1. Probe design

One of the most common errors found in probe diagnostics is the use of excessively large probes which introduce plasma density and EEDF perturbations beyond those normally accounted for in probe theory. The practice of using large probes to obtain a 'good-looking' probe characteristic (one with a clearly expressed saturation in electron and ion current) has erroneously established the Langmuir probe as an intrusive diagnostic method. To be truly non-intrusive, as it is when it is used properly, the probe must be small enough so as not to affect the ionization and energy balance and the discharge current distribution in the surrounding plasma. Note that not only the collecting tip of the probe but also the insulated probe holder adjacent to the probe tip should be sufficiently small. A very general requirement for Langmuir probe application and validity of the Druyvesteyn formula is collisionless electron motion about the probe

$$a,\ b,\ \lambda_D \ll \lambda_e \tag{1}$$

where a and b are the probe tip and probe holder radii respectively, λ_D is the Debye length and λ_e is the electron mean free path. When this inequality is not satisfied, the plasma density is depleted around the probe since electron diffusion from the surrounding plasma cannot compensate electron collection by the probe [5] and this condition leads to significant distortion in the low-energy part of the EEDF [6]. Another kind of EEDF distortion by large probes can occur when the generation rate of high-energy electrons due to electron–electron interaction in the surrounding plasma is too low to compensate for the loss of high-energy electrons to the probe [7]. In low-density and high-electron-temperature plasmas this may appear as depletion of the EEDF tail.

In a probe designed for RF discharge diagnostics, special care should also be taken to prevent electrical contact between the probe tip and any sputtered conductive layer on the insulated probe holder [8]. This may cause unpredictable increases in the probe collecting area and it may finally result in an exaggerated value of plasma density being inferred from the probe measurement.

2.2. Probe contamination

Probe contamination is a very common problem in probe diagnostics of DC discharges and it becomes especially critical in EEDF measurements [2]. In RF discharges this problem becomes even more severe due to

sputtering of the RF electrode constituents. Contamination of the probe tip with low-conductivity layers introduces additional resistance into the probe circuit that leads to severe distortion at the peak in the measured second derivative of the probe characteristic. This distortion appears as a suppression, or even as an absence, of low-energy electrons in the measured EEDF.

Another contamination problem is the extremely high sensitivity of the probe work function to the condition of the probe surface, particularly the probe temperature. Instability in the probe work function due to a change in probe current (and so also in probe temperature), or a change in the probe surface condition due to continuous sputtering of the RF electrode, result in distortion of the probe characteristics since under such conditions the probe sheath voltage does not correspond to the applied probe voltage. During probe measurement, hysteresis in the probe characteristic and its derivative usually indicates a change in probe work function [2]. This generally occurs when the probe sweep time is comparable to the characteristic time constant for a change in work function ($\tau_{wf} \approx 1$ s). An effective remedy to probe contamination is continuous probe cleaning (by ion bombardment or by excessive electron current heating) together with a probe voltage scanning time that is much smaller than τ_{wf}.

2.3. Probe circuit resistance

Since the discharge electrodes are usually a part of the probe current path, it is important that their differential resistance R_e for probe current be much smaller than the differential resistance R_p of the probe sheath. There is a fundamental difference between RF and DC discharge electrode systems which imposes significantly harsher restrictions on the relation between the probe and the electrode areas for probe measurements in RF plasmas [4]. In DC discharges the conduction current through the electrode (anode or cathode) sheath is equal to the discharge current and the differential resistance of the electrode sheath (which participates in the probe circuit) is usually negligibly small when compared with the minimal differential resistance of the probe sheath. This is not true in RF discharges where conduction currents to the RF electrode sheaths are much smaller than the RF discharge currents. Therefore, at an equal plasma density (i.e. similar RF and DC discharge currents and similar probe currents) the differential DC resistance of the RF electrode sheath is much higher than that of a similar DC discharge. Thus the DC resistance of the RF electrode sheath R_e can be comparable to the probe sheath differential resistance R_p and can thereby lead to distortion in the measured EEDF of an RF plasma. This distortion is most prominent in the low-energy part of the measured EEDF, since $R_p = (dI_p/dV_p)^{-1} \approx T_e/I_p$ has its minimum value when the probe potential is equal to the plasma potential. Thus, $R_{pmin} \approx T_e/I_{e0} \propto T_e^{1/2}/n$, where I_{e0} is the electron saturation current to the probe. The worst situation occurs when the EEDF has a two-temperature structure, such as in the case of a low-pressure RF discharge in a Ramsauer-type gas [9]. In this case R_{pmin} is governed by the low-temperature electron group with temperature T_{e1}, while the DC floating voltage on the RF electrode makes the electrode accessible to only the high-temperature electron group with temperature T_{e2} ($T_{e2} \gg T_{e1}$), and consequently R_e is governed by T_{e2}. To neglect the RF electrode resistance, the ratio between the collecting probe area A_p and the reference RF electrode area A_e must be extremely small, i.e.

$$A_p/A_e \ll (m_e T_{e1}/M T_{e2})^{1/2} n_e/n_0 \qquad (2)$$

where m and M are the electron and ion masses and n_e and n_0 are the plasma density at the plasma–electrode sheath boundary and at the probe location, respectively. Assuming a 3% distortion in the second derivative measurements (which corresponds to $R_e = 0.01\ R_{pmin}$) [2] and using data obtained in an argon RF discharge [9] ($n_e \approx 0.1 n_0$ and $T_{e1} \approx 0.1 T_{e2}$), the ratio required to satisfy equation (2) is $A_p/A_e \leqslant 10^{-6}$, which is difficult to achieve without an extremely large electrode area.

The EEDF distortion discussed here can be introduced by any additional stray resistance in the probe measurement circuit if it is comparable to R_{pmin}. For RF discharge probe diagnostics, an additional DC resistance can sometimes be inadvertently introduced by the probe circuit elements. Specifically employed to prevent RF disturbance of the probe sheath, miniature RF filters may introduce a DC resistance of about 10 Ω which can be comparable to R_{pmin} for RF discharges in the γ regime, where extremely large plasma densities and extremely small electron temperatures are typical [10]. To our knowledge, the issue of probe circuit resistance has never been properly addressed for EEDF measurements in RF systems.

2.4. RF distortion

RF interference with the probe sheath is a very common problem for all probe measurements in RF plasmas. The widely held opinion that the ion part of the probe characteristic and double-probe characteristics are not affected by RF distortion is not true [11]. The nature of the problem stems from RF oscillation of the plasma potential with respect to ground and the nonlinearity of the probe sheath. Due to RF voltage rectification in the probe sheath, these conditions result in distortion of the probe characteristics and, to an even larger extent, of their derivatives. The issue of RF distortion and its elimination in EEDF measurements has been discussed by many authors [2, 4, 11–22] and partial solutions to the problem have been achieved by some. Among the approaches suggested to reduce RF distortion are: a tuned RF filter in the probe circuit to increase the input impedance of the probe measurements circuitry [11–13, 17, 21, 22] and biasing the probe with RF voltage having the correct phase and amplitude to minimize the RF potential across the probe sheath [15, 19]. Such procedures have been usually performed for the fundamental driving frequency of the RF discharge and in some cases for the second harmonic also. However, just tuning a

filter, or filters, or adjusting the probe RF bias does not guarantee that RF distortion is absent, or at least negligible. This procedure only attains the minimum level of distortion for a given probe circuit design. As shown experimentally [13] in a quiescent DC plasma by applying a controlled RF voltage with amplitude $\phi_{p\sim}$ into the probe sheath, the relation $\phi_{p\sim} \leqslant 0.5\,T_e$ must be satisfied to neglect RF distortion in EEDF measurements. For a non-Maxwellian EEDF, one should use the minimal electron 'temperature' T_{emin}, taken from the steepest part of the function $\ln I''(V_p)$. To achieve undistorted measurements of the EEDF in RF plasma, a relationship between the probe–plasma impedance Z_{sh} and the external probe circuit impedance Z_c must be fulfilled [13]

$$Z_{sh}/Z_c \leqslant 0.5\,T_{emin}/V_{p\sim} \tag{3}$$

where $V_{p\sim}$ is the peak plasma RF voltage referenced to ground. It is essential to note that due to the nonlinear interaction of the RF driving voltage with the RF electrode sheaths, the plasma potential consists of the fundamental frequency ω and also some harmonics which may be of considerable amplitude. Therefore, to achieve undistorted measurements, equation (3) must be satisfied for all frequency components of the plasma potential.

In RF discharges the probe impedance is mainly determined by the probe plasma capacitance C_p which is the total probe capacitance including the probe holder and any intentionally added shunting capacitance [12]. Shunting capacitance is added to increase the coupling between the probe and the RF plasma and thereby to lower the extremely high, normally unachievable, requirement prescribed in equation (3) for probe circuit (actually RF filter) impedance. Thus, the following condition must be satisfied for each harmonic κ of the plasma potential $V_{p\kappa\sim}$ to avoid RF distortion in the EEDF measurement:

$$Z_{c\kappa} \geqslant 2\,V_{p\kappa\sim}/\kappa\omega C_p T_{emin} \qquad \text{for } \kappa = 1, 2, 3\ldots \tag{4}$$

where κ is the harmonic number, $Z_{c\kappa}$ is the RF filter impedance at frequency $\omega\kappa$ and $V_{p\kappa\sim}$ is the amplitude of the κth harmonic component of the RF plasma potential. To our knowledge, condition (4) has never been shown to be satisfied in any probe diagnostic experiments in RF discharges to date.

2.5. Low-frequency noise and drift

Low-frequency plasma potential noise and drift, mainly due to instability in the RF supply voltage, can cause distortion in the probe characteristics similar to RF distortion. This problem is known for DC discharges [2]. However, it is much more serious in RF discharges, since in the latter a large DC voltage usually exists between the plasma and the RF electrodes which serve as a reference electrode in the probe circuit. This DC voltage can be of the order of the RF voltage applied to the RF electrodes and may reach hundreds of volts. Therefore, even a 1% instability (ripple or drift) in the RF driving voltage can be a source of probe voltage noise and drift, which may be comparable to, or larger than, the electron temperature, thus introducing intolerable distortion into the measured probe characteristic. Instability in the plasma potential becomes particularly critical for EEDF measurements in RF discharges in the γ mode, where driving voltages can be over a few hundred volts and electron temperature can be less than 0.1 V.

Apart from distorting the probe characteristic by a high level of noise, even a small low-frequency noise, originating in the discharge itself and/or in the power supply, reduces the signal-to-noise ratio of measurements and the dynamic range of the measured EEDF (i.e. the ability to analyse the high-energy tail of the EEDF). This problem can be partially overcome by using averaging techniques [2]. Unfortunately, for a great majority of plasma experiments, the interference noise is not random and therefore using an averaging techniqc yields only limited success.

A noise-suppression feedback system [22–25] included in the probe circuit can be a radical solution to the low-frequency noise and drift problem, but such a technique has not been used in probe experiments of RF plasmas to date.

All the problems in EEDF measurements that have been discussed here usually have similar consequences and generally lead to widening and smoothing of the probe characteristic and its derivatives over the energy range in the vicinity of the plasma potential. The rounding of the second derivative $I_p''(V_p)$ at its peak and the large gap ($\Delta V \geqslant T_e$) between the peak and the zero crossing of the second derivative, are usually signs that one, or more, of the above-mentioned problems are taking place. In this case the measured EEDF appears to be depleted in low-energy electrons and the mean electron energy deduced from this measurement appears to be excessive.

2.6. Probe characteristic processing

Historically, the first attempts to find an EEDF from the Druyvesteyn formula were through graphical differentiation of the electron part $I_e(V_p)$ of the probe characteristic $I_p(V_p)$. The function $I_e(V_p)$ was found as the difference between the measured $I_p(V_p)$ and an extrapolated (either linearly or parabolically) ion component $I_i(V_p)$ of the probe current which was found at large negative probe voltages where $I_e(V_p)$ was assumed to be negligible. Such a procedure is reasonable for inferring the electron current corresponding to the main body of electrons with energies close to the average energy, but it is inappropriate for defining $I_e(V_p)$ corresponding to the high-energy tail of the EEDF since $I_e(V_p)$ found in this way is a small difference between two large quantities $I_p(V_p)$ and $I_i(V_p)$ both of which are known with only limited accuracy. With this approach a huge magnification in the error resulting from differentiation of this difference makes it meaningless to analyse electrons with energies higher than the floating potential $|V_f| \approx (3\text{–}5)\,T_e$.

Only about 30 years after the Druyvesteyn formula was published, a breakthrough in processing probe data was made with the introduction of an AC measuring (or

probe modulation) technique based on the nonlinear interaction of a small AC or RF voltage with the probe sheath. Today, together with the pulse measuring technique, the AC measuring technique has become one of the main methods for measuring the EEDF [2]. One common basis for both techniques stems from the fact that over a large, although limited, range of probe voltage the second derivative of the ion current I_i'' is much smaller than that of the electron current I_e'', i.e. $I_e'' \approx I_p''$. This allows one to differentiate the total probe characteristic without dubious assumptions about the functionality of the ion current. Following such an approach, a great number of experimental EEDF studies have been performed in different kinds of gas discharge plasmas over the last 30 years. However, at large negative probe voltages I_i'' becomes comparable to I_e'' and puts an upper limit on the dynamic range (or energy interval) where an EEDF can be reliably inferred from probe measurements.

Recently, ubiquitous application of computers and a deep faith in curve-fitting techniques have promoted a reincarnation of the previously rejected manipulation with ion current. Thus in recent works on EEDF measurements in RF discharges the ion current (at all discharge conditions) is fitted parabolically, i.e. $I_i(V_p) \propto |-V_p|^{1/2}$ corresponding to the Langmuir orbital-motion-limited (OML) theory. Apart from the inaccuracy introduced by 'differencing methods' and the error magnification due to the differentiation that follows, the OML theory itself has many assumptions which are difficult to satisfy under actual experimental conditions. The following are some of these assumptions along with comments:

(i) A small probe and rare plasma, $a \ll \lambda_D$ (λ_D is the Debye length).
(ii) No ion collisions in the probe sheath, $\lambda_D \ll \lambda_i$ (λ_i is the ion mean free path). Note, that orbital motion is extremely sensitive to (and destroyed by) ion collisions.
(iii) Cold ions in the surrounding plasma. Indeed in some cases, the ion energy in the plasma can be close to the mean electron energy.
(iv) A Maxwellian EEDF. Generally, ion current to the probe depends on the EEDF.
(v) One-dimensional cylindrical probe sheath. At high probe voltage the shape of the sheath around the cylindrical probe tip approaches spherical for which OML theory gives $I_i(V_p) \propto |-V_p|$.

Note also that the ion current to the probe depends on the particular ionization process in the surrounding plasma.

The accuracy of OML theory or even the more sophisticated Laframboise theory [26] which differs from OML theory by accounting for the final ratio of a/λ_D and T_i/T_e, has been questioned in many works [27–29]. Although a parabola can be fitted to represent practically any ion current dependence, there is no proof that the chosen fit precisely describes the ion current behaviour in the region where it is extrapolated. For either flat, cylindrical or spherical probes, this is a matter of luck in the choice of an appropriate probe voltage range. An example of a mistakenly recognized OML regime can be found in recent work [21] where the ion current ideally fits a parabola over a large interval of probe voltage while the probe sheath is in an apparently RF-distorted and collison-dominated regime.

In many recent works on EEDF measurements in RF discharges the use of parabolic fitting for ion current makes the results questionable, at least in the high-energy part of the EEDF where the results are so sensitive to the assigned functionality of $I_i(V_p)$. In this same context, the extremely large dynamic range (over six or more orders of magnitude) of the reconstructed $I_e''(V_p)$ found in some recent works seems to be overly optimistic.

Indeed, the dynamic range of an EEDF measurement is limited by the ion current contribution which is of maximal influence for light gases and small ratios of a/λ_D [30]. For $a/\lambda_D < 1$, ion motion in the probe vicinity can be considered to be close to the OML regime with $I_i(V) \propto |-V|^{1/2}$ and corresponding calculations can be used as a 'worst-case' estimate of uncertainty limit for EEDF measurements [2]. Thus, the dynamic range of second-derivative measurements limited by the ion current influence is defined as the ratio between maximal (extrapolated) value of I_p'' at $V_p = 0$ and I_p'' at $|V_p| \gg T_e$ for which $I_e'' = I_i''$ is about 10^4 for helium ions. For a Maxwellian EEDF, this dynamic range corresponds to the maximal electron energy $\varepsilon_{max} = 9eT_e$. This means that for an uncertainty threshold at $\varepsilon = \varepsilon_{max}$, the measured EEDF may be overestimated by a factor of no more than two.

2.7. Undefined RF discharge conditions

All results published in the last decade on EEDF measurements in RF plasmas were performed in plasma processing devices or in experimental arrangements very similar to processing reactors. The discharge conditions in these experiments were characterized by the separation L between the powered and the grounded parallel-plate electrodes and by the transmitted RF power measured in the cable connecting the RF power source to the matching network located between a power meter and the discharge reactor. This method of measuring RF power assumes that the matching network is a lossless impedance transformer and it implies that the measured transmitted RF power is equal to the power dissipated in the discharge. Indeed, as has been proven in many works (see for example [31, 32]), the RF power losses in the matcher itself, in the connecting wires and in the reactor hardware can account for more than 90% of the total measured power. Due to the nonlinearity in the electrical characteristics of the RF discharge, the power dissipated there is not even proportional to the measured transmitted power. Moreover, in low-pressure, high-voltage RF discharges almost all RF discharge power (up to 95%) may go to ion acceleration in the RF electrode sheaths [33]. Thus, for the reasons mentioned above, it seems that in EEDF measurements the characterization of RF discharge conditions by transmitted RF power measurements is irrelevant since *a priori* an unknown (possibly negligibly small)

fraction of the total measured RF power is related to the electron heating process which governs the EEDF.

Another source of uncertainty in discharge (to be precise, in the plasma) conditions is an undefined plasma volume due to plasma diffusion and discharge current branching out of the discharge gap towards the grounded discharge chamber walls. This occurs in asymmetrically driven RF discharges with a powered and a grounded electrode of equal area and to even a much larger extent in typical plasma processing devices where the grounded wall works as the main grounded electrode. In this last case the RF plasma volume depends on RF power, gas type and gas pressure, and chamber geometry. Thus it is poorly correlated with the actual electrode gap L.

Due to uncertainties in electron heating power, plasma volume and discharge conditions, previous EEDF measurements in RF plasma appear to be poorly defined. Thus it is nearly impossible to relate measured EEDFs to a precise discharge condition (discharge power density or current density) and to compare results obtained with different reactors and matching systems. The problem of characterization of the basic electrical parameters of RF discharges (current, voltage and especially discharge power) as well as plasma topology uncertainty still remains an important concern in the plasma processing community.

3. Experimental probe system

3.1. Apparatus and measurement procedure

To address the problems listed in the previous section, we have assembled an experimental probe measurement system arranged as shown schematically in figure 1. This probe measurement system complements our experimental system for RF discharge studies [34, 35]. The arrangement is a modification of a previously developed noise-suppression probe circuit with fast pulse measurement of the probe characteristic followed by direct analogue differentiation and digital signal processing [25]. Shown in figure 1, the probe diagnostic–RF system mainly consists of: a radially confined, symmetrically driven RF discharge chamber with Langmuir probes at the midplane, resonant RF filters to prevent RF distortion, a probe measurements circuit with noise suppression and discharge resistance compensation feedback, a probe voltage generator, an analogue filter–differentiator, an ensemble averaging device and a PC for data processing and calculation of the EEDF integral-based quantities such as the plasma density n_0, the mean electron energy $\langle\varepsilon\rangle$ and the effective electron temperature $T_{eeff} = 2\langle\varepsilon\rangle/3e$.

The pulse measuring technique [2] is adapted here to measure and differentiate the probe characteristic. In this technique the probe voltage is swept linearly in time ($V_p = \alpha t$) for a few milliseconds or less to keep the probe temperature constant and thereby avoid a change in the probe work function during the probe voltage sweep. Under this condition the second derivative of the probe current with respect to voltage is proportional to the

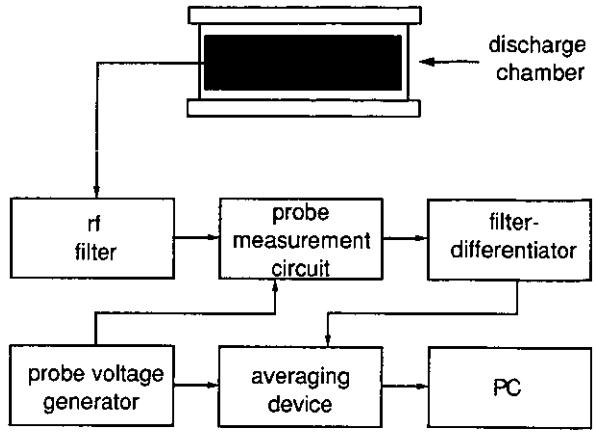

Figure 1. Functional diagram of the EEDF measurement system.

second derivative of the probe current with respect to time through $I''(V) = \alpha^{-2} I''(t)$. Differentiation of the probe current signal is performed by an analogue filter–differentiator consisting of two differentiating amplifier stages and three Bessel-type two-pole low-pass filters. The filters are placed at the input and the output of the filter–differentiator and between the two differentiating stages. The filter bandwidth may be conveniently switched so as to be appropriate for the discharge conditions. The probe voltage sweep rate can be varied between 8 and 200 $V\,m\,s^{-1}$ and is generally chosen as a compromise between high energy resolution and high signal-to-noise ratio. The differentiator gain is also variable and calibrated for each position of a switch. The filtered output of the probe current $I_p(t)$ and its derivatives $I'_p(t)$ and $I''_p(t)$ can be monitored on the scope face of the digitizer as shown in figure 2. In conjunction with the built-in gain variability of the stages, the real-time signal monitoring makes it possible to adjust the signal levels in each stage of the filter–differentiator to keep signals small enough not to overload the differentiator and the digit-

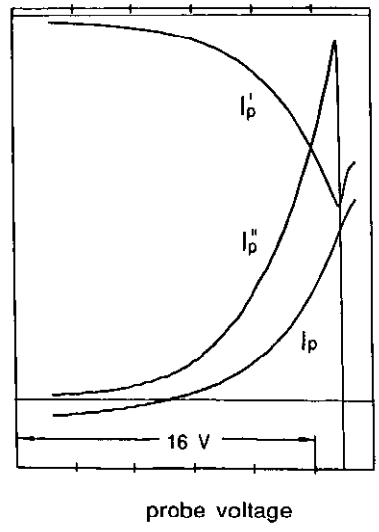

Figure 2. Typical traces of the probe current/voltage characteristic, I_p, its first derivative I'_p and its second derivative I''_p in a helium RF discharge with $p = 0.1$ Torr, $L = 6.7$ cm and $V_d = 140$ V.

izer, yet large enough to attain the highest possible signal-to-noise ratio.

The second-derivative signal $I_p''(t)$ is ensemble averaged in an Analogic Corp., Data 6100, waveform analyser (WFA) working in a compressed 12-bit A/D conversion mode. Each averaged $I_p''(t)$ is usually based on 1000 probe sweeps and each digitized record has either 256 or 512 points. Depending on the number of averages and the number of digitized points per sweep, the total acquisition and averaging time for one averaged second derivative curve takes only 1–2 min. Because of the short time necessary to make a complete measurement, inaccuracy due to slow drift in plasma parameters (which is typical in gas discharges) is significantly reduced.

The instantaneous and averaged $I_p''(t)$ are proportional to the electron energy probability function (EEPF) or $f(\varepsilon)$ (where $f(\varepsilon) = F(\varepsilon)\varepsilon^{-1/2}$), which can be monitored on the WFA screen in linear ($\times 1$, $\times 10$ or $\times 100$), and also in logarithmic scale, practically in real time, thus providing indispensable flexibility in the EEDF measurements and in adjusting the probe measurement system. The averaged second derivative can be stored in the WFA and, after transfer to a PC, used for further processing and plasma parameter calculations. Signal processing includes re-scaling and coordinate shift and flip-over with respect to the plasma potential. Calculation of the EEDF and its integrals n_0 and $\langle\varepsilon\rangle$ are as follows

$$F(\varepsilon) = 2(e^2 A_p)^{-1}[(2m/-e)V_p]^{1/2} I_p''(t)\alpha^{-2} \qquad -eV = \varepsilon$$

$$n_0 = \int_0^{\varepsilon_{max}} F(\varepsilon)\,d\varepsilon \qquad \langle\varepsilon\rangle = n_0^{-1}\int_0^{\varepsilon_{max}} \varepsilon F(\varepsilon)\,d\varepsilon$$

where e and m are electron charge and mass, V_p is the probe potential referenced to the plasma potential, the plasma potential is found from the zero crossing of $I_p''(V)^2$ and ε_{max} is the maximum electron energy corresponding to the dynamic resolution threshold in the I_p'' measurements determined by noise or by the influence of the ion second derivative. Since, $\varepsilon_{max} \gg \langle\varepsilon\rangle$, the calculated values of n_0 and $\langle\varepsilon\rangle$ are insensitive to the particular value of ε_{max}.

3.2. Probe measuring circuit

The probe measuring circuit (PMC) is shown in figure 3. Op-amp OP_2 drives the RF discharge electrodes with the probe sweep voltage while measurement probe P_1 is grounded through the current-to-voltage converter, OP_1. The floating-loop probe P_2 is in the same plane as P_1 and senses DC and low-frequency components of the plasma potential. Being connected to the negative input of op-amp OP_2, the probe P_2 introduces the plasma potential in opposite phase into the probe circuit, thereby cancelling low-frequency noise and the large DC voltage drop in the RF electrode sheaths. The loop probe P_2 also has another important function of RF-coupling the measuring probe P_1 to the plasma so as to make probe P_1 follow the RF plasma potential (see next section).

Thus, independent of the rectified voltage between the RF electrode and the plasma, the measurement probe P_1 is automatically biased by the probe driver OP_2 so that

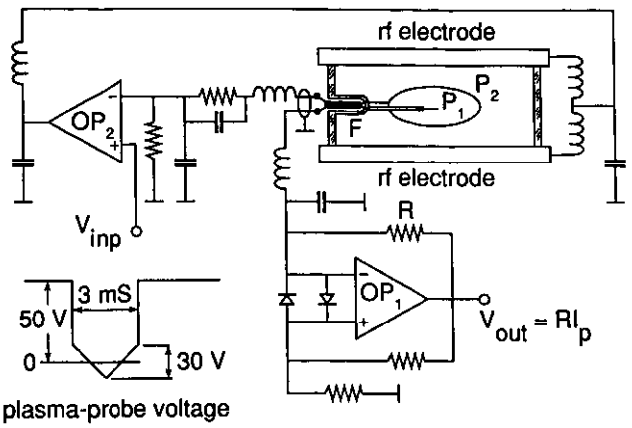

Figure 3. Simplified diagram of the probe measuring circuit.

the voltage difference between probe P_2 and ground is, with a high degree of accuracy, equal to $10V_{inp}$, where V_{inp} is the driver input voltage referenced to ground and 10 is the driver gain determined by the RC voltage divider at the negative input of OP_2. Note that the feedback system cancels any voltage between the reference probe P_2 and the output of OP_2 (connected to the RF electrodes), including voltage drift and voltage drop across the highly resistive RF electrode sheaths due to probe current (provided that the voltage spectrum is within the probe driver's bandwidth). The probe driver OP_2 (PA 88 of Apex Microtechnology Corp.) supplies up to 400 V with a maximum probe current of 50 mA and has a 30 kHz small-signal bandwidth that practically eliminates DC drift (80 dB suppression) and low-frequency noise within the operational spectrum of the filter–differentiator having a bandwidth of 8 or 20 kHz.

The noise compensation circuit, however, does not cancel the voltage drop localized between the measurement probe P_1 and ground that is due to the DC resistances of the RF filters F and the RF filtering choke at the input of the current-to-voltage converter OP_1. The uncompensated probe circuit resistance R_c is about 20 Ω and in some discharge regimes it may be comparable to the minimum value of probe differential resistance R_{pmin}, thereby resulting in distortion at the low-energy part of the EEDF. This effect is demonstrated in figure 4 where the second derivative of a Maxwellian EEDF is shown as a function of normalized probe voltage calculated with different values of the parameter $\delta = R_c/R_{pmin}$. Distortion is evident even for a small uncompensated circuit resistance ($\delta = 0.1$), leading to a decrease in the low-energy part of the EEDF and giving the appearance of an increased electron temperature. To avoid this problem, the probe current-to-voltage converter is designed to be a gyrator [36] having a negative input resistance equal to R_c that develops at the converter input a voltage equal but opposite in phase to the voltage drop across R_c. Thus for all probe currents the measurement probe appears to be at ground potential.

The waveform of the probe voltage is introduced to the positive input of the driver from the probe voltage generator and after being amplified ten times it is applied

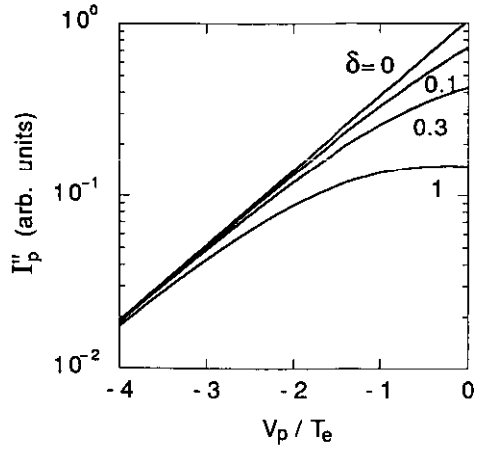

Figure 4. Second-derivative distortion due to final probe circuit resistance R_c. Here the second derivatives are shown as functions of the normalized probe voltage V_p/T_e for different values of the parameter $\delta = R_c/R_{pmin}$.

to the RF electrodes as shown in figure 3. A typical time and voltage scale of the probe (actually the RF electrode) waveform is shown in the inset of figure 3. The ramp pulse consists of a linearly rising and falling part. This is a particularly convenient diagnostic option since many different potential problems associated with electronics and with discharge instabilities can be revealed by comparing the probe current sweep in both directions. Continuous probe tip cleaning is achieved through ion bombardment by negatively biasing (30–60 V) the measurement probe in the time interval between ramp pulses. In the present experiment, this continuous cleaning technique appears to be the only way to maintain a clean probe in high-voltage RF discharges with high sputtering rates (such as in a γ discharge) where, without cleaning, the probe can be contaminated in a few seconds.

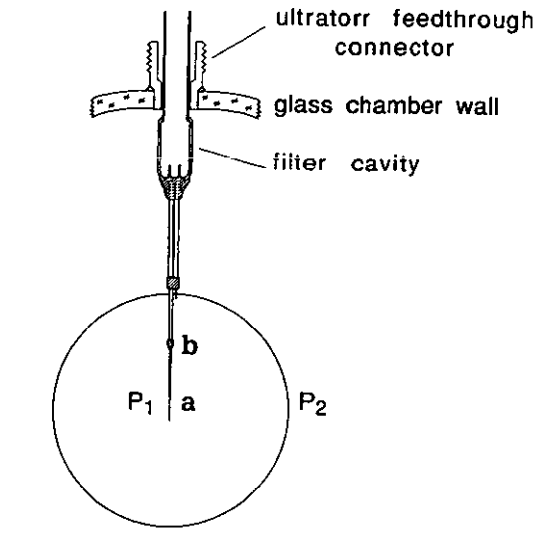

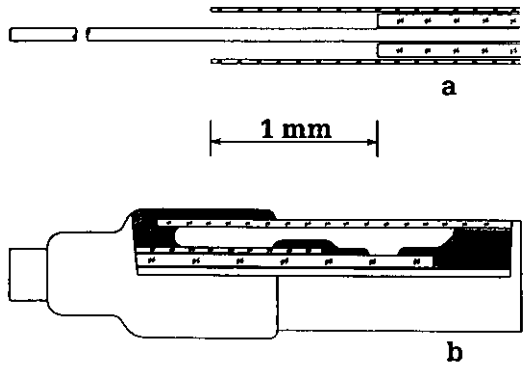

Figure 5. Probe system. The positions a and b are given magnified at the bottom to show a shielding sleeve (position a) and epoxy vacuum seals (cross hatched, position b).

3.3. Probe design

The probe system used in this experiment is shown in figure 5. It consists of a small measurement probe (P_1 in figure 3) and a wire loop reference probe P_2. Both probes are placed in the midplane of the discharge gap and are introduced into the midplane of the discharge chamber via an ultra-torr vacuum feed-through sealed into the glass chamber wall. The probes are designed to avoid significant perturbation of the plasma up to the highest gas pressures used in our work ($p \leqslant 3$ Torr).

Probe P_1 is a cylindrical tungsten rod, 6.3 mm in length and 38 μm in radius, with a capillary sleeve preventing electrical contact between the tip and any conductive sputtered material on the probe holder. To prevent plasma perturbation, the holder radius is made smaller than the electron mean free path λ_e at all gas pressures where the probe is to be used. The reference probe P_2 is a thin (127 μm in radius) tungsten wire with a 30 mm loop radius. The reference probe dimensions and shape are a compromise between small plasma distortion in the vicinity of the probe and a large surface area for better coupling to the plasma. The reference probe P_2 has two diverse functions. For DC and low frequency, it senses plasma potential and introduces the feedback into the noise-suppression circuit (OP_2 in figure 3) while for RF (mainly for the second harmonic in a symmetric discharge), P_2 is coupled to the probe P_1 via small capacitor and thus it markedly improves the coupling of P_1 to the plasma so as to make P_1 follow the RF plasma potential and, as mentioned earlier, reduce the stringent requirement on the input RF impedance of the probe circuitry. To perform these functions the reference probe must be situated so as to be equipotential (for RF) with the measurement probe.

Both probes are supported by two 0.5 mm diameter nickel rods covered by insulating capillary tubes of 0.7 mm diameter and are sealed with epoxy to the RF filter cavity. The filter assembly plugs onto the probe wires extending from the capillaries. A detailed drawing of the junction of the measuring probe and the rods and of the vacuum sealing points is shown in figure 5.

3.4. RF filter design

Miniature RF filters for the measurement probe and the reference probe have been designed to avoid RF distortion. The filters are inserted into a glass cavity that is surrounded by plasma and that is in the same RF equipotential plane as the probe wires (see figure 3). Having filters within the plasma minimizes the RF coupling between the probes and ground. The RF filter cavity is sealed in a 0.25″ Kovar tube which is affixed to the glass discharge chamber wall via a vacuum feedthrough connector as shown in figure 5. The RF plasma potential $V_{p\sim}$, its frequency spectrum and the reference probe capacitance to the plasma have been studied in an argon RF discharge at 13.56 MHz [18] and the design of the RF filters used here is based on this work. Measurements over a wide range of discharge conditions showed that for a symmetrically driven RF discharge the total capacitance of the reference and measurement probe is about 5–15 pF depending on discharge conditions, and $V_{p\sim}$ is about 10% of the RF driving voltage [18]. Typical spectra of the plasma RF potential are shown in figure 6 for a symmetrical and an asymmetrical RF driving voltage of about 100 V. As seen in figure 6, the symmetrically excited RF discharge appears to have a significant second harmonic and small components of the fundamental and the fourth harmonic, while the asymmetric discharge has a large fundamental, a second harmonic equal to that in the symmetric discharge and small components of the fourth and the sixth harmonic. Thus, the asymmetrically driven RF discharge has almost an order of magnitude higher RF plasma potential than that in a symmetrically driven discharge. Note that for asymmetrically driven RF discharges with unequally powered and grounded electrode areas (typical for plasma processing devices) a considerable level of odd harmonics should be expected, although the fundamental harmonic may be smaller than that for a discharge having equal-area electrodes. Therefore, RF filtering that is adequate for a symmetrical discharge could be inadequate for an asymmetrical discharge and vice versa in some cases.

In our filter design we have combined a resonant filtering technique (tuned probe) proposed by Gagne and Cantin for a symmetrically driven RF discharge at 3.5 MHz [12] and a resistive filter technique used in our earlier measurements in RF discharges at 40 MHz [11]. To achieve maximum filter impedance we employed microminiature (1.8 mm diameter × 6.2 mm length) chokes with a self-resonance at 13.5 and 27 MHz for probe P_1 and microminiature (1.2 mm × 4 mm) resistors for probe P_2 as shown in figure 7(*a*). The filters are positioned as shown in figure 3. They are connected to the probe tips via a microconnector making filter replacement easy and simplifying adjustment and experimentation with different kinds of RF filter. The filter impedance versus frequency for the two filters in parallel is shown in figure 7(*b*). The two resonances correspond to the fundamental (which originates from a small imbalance in the RF matcher) and the second harmonic. Since probe sheath impedance decreases with frequency and the filter bandwidths are fairly broad (low Q factor of the filter system, $Q \approx 10$), the ratio between the filter and

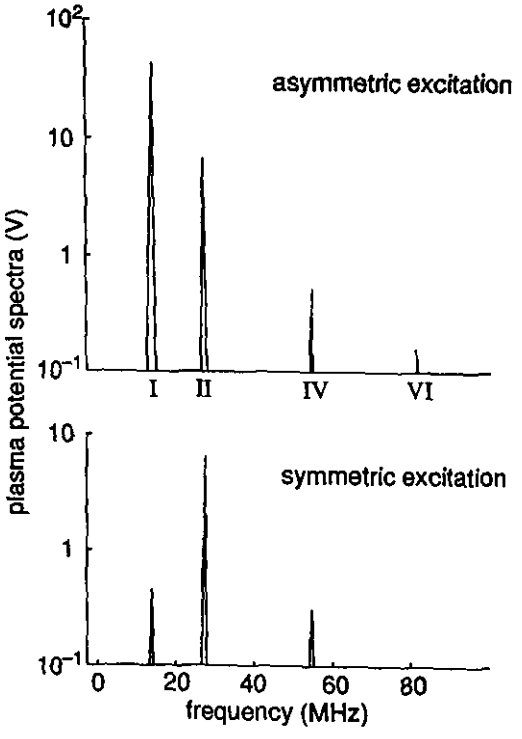

Figure 6. Plasma potential spectra for asymmetric and symmetric RF discharge [18].

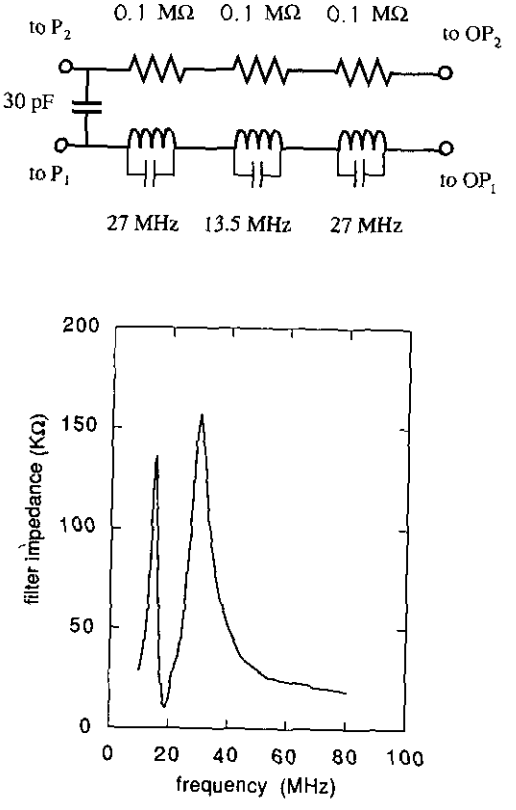

Figure 7. Probe filter diagram and its impedance/frequency characteristic for resistive and resonant branches connected in parallel.

the probe impedance is sufficient also to remove higher-order harmonics. Knowing the filter impedance for the largest (second) harmonic ($Z_{2\omega} = 1.6 \times 10^5\,\Omega$) and the probe capacitance for the largest discharge voltage ($C_p \approx 15$ pF), the ratio between the discharge voltage V_d and the minimal electron temperature T_{emin} can be obtained from equation (4) for which an undistorted probe measurement in a symmetrically driven RF discharge is possible

$$V_d/T_{emin} \leqslant 10\,Z_{2\omega}C_p\omega \approx 2 \times 10^3. \qquad (5)$$

This requirement is fulfilled in our experiments in argon over a range of RF powers between 0.02 and 100 W and over a range of gas pressure between 3 mTorr and 3 Torr. This requirement is also satisfied in helium over a wide range of powers and gas pressures except maybe for two extreme conditions: the first of these is in the γ regime at a relatively large gas pressure ($P \geqslant 1$ Torr) where the electron temperature abruptly drops reaching values close to room temperature; the second of these is a high voltage ($V_d \approx 1$ kV) RF discharge at the lowest possible gas pressure (near extinction, when the two RF sheaths nearly overlap). This discharge regime has the largest electron temperature and the smallest plasma density, whereby it presumably has a prove capacitance C_p that may be too small to provide coupling adequate for the probe system to follow the RF plasma potential.

3.5. Practical considerations

A most informative and convenient way to represent an electron energy spectrum is to directly display the measured second derivative I_p'' as a function of the probe voltage referenced to the plasma potential eV_p on a semi-logarithmic scale because I_p'' is proportional to the electron energy probability function (EEPF), $f(\varepsilon)$. The log I_p'' versus V_p allows observation of the EEPF over a large dynamic range and it is easily compared with a Maxwellian distribution (a straight line in this representation). This representation also allows one to observe the second derivative near its maximum and zero-crossing point which is the plasma potential [2]. More importantly, the energy difference (Δ) between the peak and the zero crossing of I_p'' is a sensitive indicator of the overall quality of the experiment since, as mentioned previously, low-frequency and RF interference, probe contamination and stray resistance in the probe measurements circuit, and plasma density depletion around large probes and at high gas pressures, all lead to suppression of the peak in I_p'' and to widening of Δ. Even if all these issues are properly addressed, a small 'residual' gap (for a good-quality experiment $\Delta < eT_{emin}$) usually occurs and I_p'' must be extrapolated to avoid a hole in $f(\varepsilon)$ at small energy. This 'residual' gap is probably a consequence of electron reflection, secondary-electron emission, inhomogeneity of the probe work function along the probe collecting surface and the convolution effect usually accompanying differentiation [2]. For analogue differentiation in the time domain adopted in this work, the convolution effect is caused by the limited bandwidth of the low-pass filters. The bandwidth of the filter–differentiator Ω is chosen in our set-up as a compromise between high energy resolution (a small gap between the peak and the zero crossing of I_p'') and noise limiting which affects the dynamic range (in the high-energy tail region) of the EEDF. The convolution effect is demonstrated in figure 8 where log I_p'' is presented for measurements with

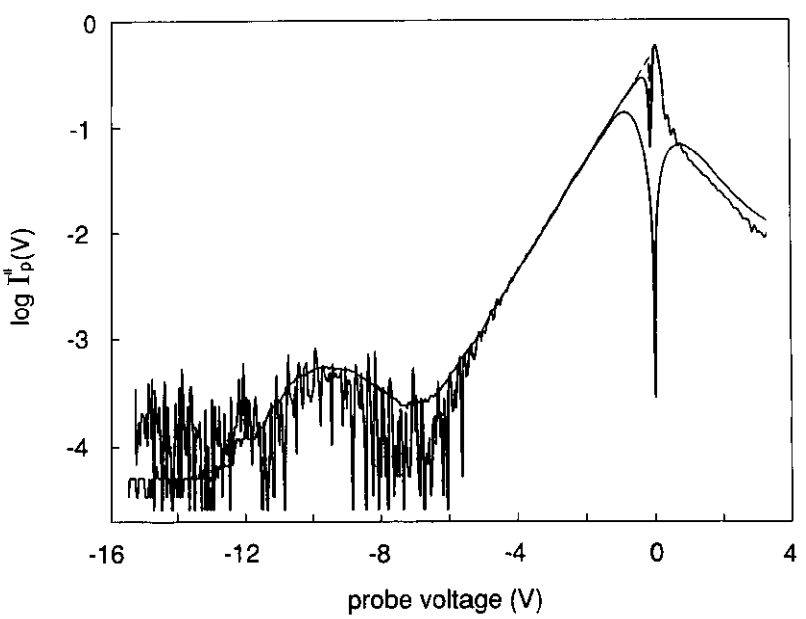

Figure 8. Second derivative versus probe voltage for different bandwidth of filter–differentiator; $\alpha = 40\,V\,m\,s^{-1}$, $\Omega = 250$ kHz (noisy curve) and $\Omega = 20$ kHz (smoothed curve). These data are obtained in the cathode glow region of a Ne–Hg arc discharge.

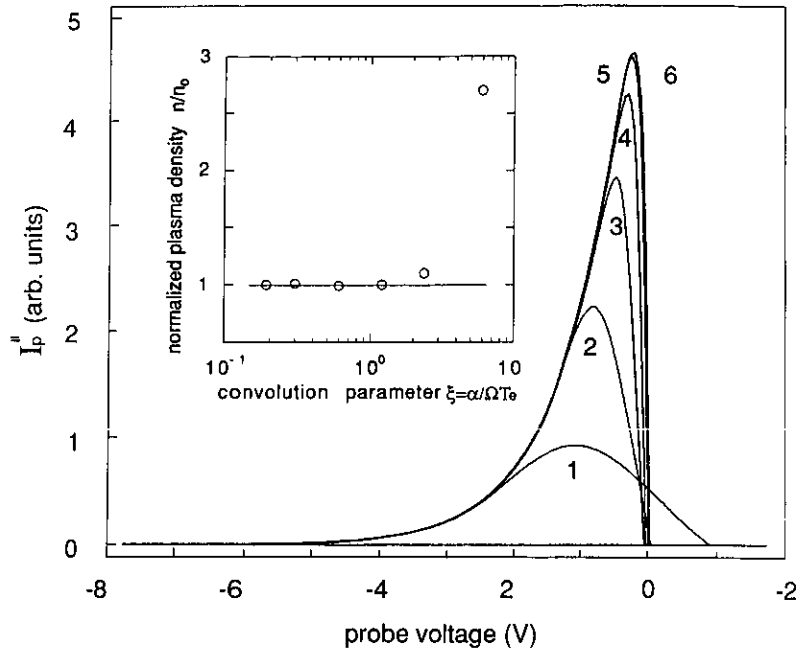

Figure 9. Second derivative and plasma density distortions due to limited differentiator bandwidth: (1) $\Omega = 8$ kHz; (2) $\Omega = 20$ kHz; (3) $\Omega = 40$ kHz; (4) $\Omega = 80$ kHz; (5) $\Omega = 160$ kHz; (6) $\Omega = 250$ kHz. Here n is the plasma density obtained by integration of convolute I_p'' and n_o is the plasma density for $\Omega = 250$ kHz when the second derivative is practically undistorted. Discharge conditions are the same as for figure 8.

different bandwidths. As the bandwidth is reduced from 250 to 20 kHz the analogue noise decreases and the dynamic range of I_p'' increases from 50 to 70 dB. At 20 kHz, digital noise is due to the limited dynamic resolution of the digital waveform averaging. Improvement in the signal-to-noise ratio, and likewise the dynamic resolution, however, incurs a sacrifice in the energy resolution, increasing the gap between the peak and the zero of I_p'', while the position of the zero crossing (plasma potential) remains practically unchanged. With better energy resolution, the trace of I_p'' for 250 kHz indicates how to extrapolate I_p''. Thus, it seems natural to extrapolate I_p'' exponentially (linearly in semi-logarithmic scale of figure 8) towards the plasma potential as shown by the broken line in figure 8. Generally, it is rare to measure an electron distribution which is coincident with a Maxwellian over so large a dynamic range as in figure 8. In a majority of cases, the electron distribution can be approximated by a Maxwellian only for its low-energy part within an energy interval close to its mean electron energy. In general, the EEDF is not Maxwellian (the slope of $\log I_p''(V_p)$ is not constant) and in this case it is unclear exactly where on the I_p'' curve one has to start the exponential extrapolation. Empirically, we have arrived at a 'deconvolution' technique (there are too many possible speculations involved in supporting this technique to discuss it seriously) where the energy of the starting point of the extrapolation is assigned to be 2Δ (to the left in figure 8) from the zero crossing of I_p''. This procedure has been programmed in the PC and is used for calculation of the EEDF and its integrals.

The effectiveness of such a deconvolution is demonstrated in figure 9 where convoluted second derivatives measured with different differentiator bandwidths are shown in a linear scale. Plasma density (which, more than $\langle\varepsilon\rangle$, is sensitive to low-energy behaviour of the EEDF) calculated using the described 'deconvolution' technique is given in the inset to figure 9. The error in the plasma density obtained from the deconvoluted second derivative is less than 10% provided that the convolution parameter, $\xi = \alpha/\Omega T_e$, is less than 2. In practice ξ is kept < 1, thus ensuring negligible errors due to the limited differentiator bandwidth. For Druyvesteyn-like distributions when the measured second derivative has a plateau (or even some decline) within small energies the procedure described above is clearly not adequate. In this case we used tangent extrapolation or, in some cases, no extrapolation. Fortunately, differences in the calculated values of n_0 and $\langle\varepsilon\rangle$ using either of these methods is no more than a few per cent.

A typical experimental result for an argon RF discharge is shown in figure 10 where the true EEDF is given in a linear scale with a magnified high-energy tail, and the EEPF is given in a semi-logarithmic scale which is more informative and convenient. In what follows we will represent our results as an electron energy probability function in semi-log scale without reconstructive extrapolation of its low-energy part. This representation (which we would like to see in others' works) allows one to rapidly judge the quality of the experiment and sometimes to recognize the possible source of error in the EEDF measurement.

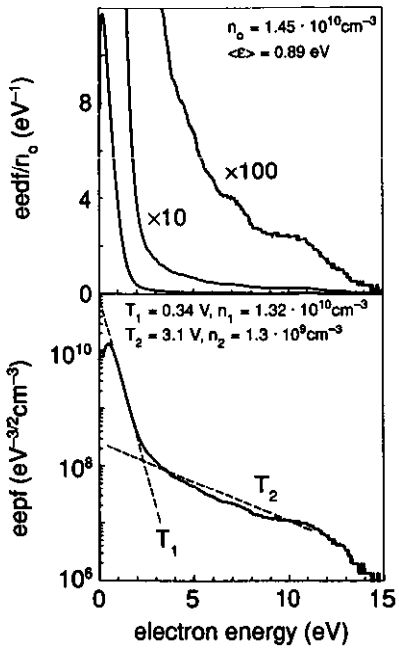

Figure 10. EEDF and EEPF measured in argon RF discharge $f = 13.56$ MHz, $p = 0.1$ Torr, $L = 2$ cm, $J = 2.65$ mA cm^{-2} [9].

The effectiveness of the probe measurement system for low-frequency noise suppression is demonstrated in figure 11. These results have been obtained in a noisy Ne–Hg DC discharge. Single probe traces corresponding to noise suppression and no suppression are shown on the left side, while ensemble-averaged probe traces with and without noise suppression are shown on the right side. This example shows how important it is to remove noise prior to averaging to avoid distortion in the second-derivative measurements.

The effect of RF distortion caused by the second harmonic (neglected in a majority of probe experiments in RF plasmas) is shown for a He RF discharge at 13.56 MHz in figure 12, here the fundamental harmonic is compensated due to the symmetry of the discharge itself. Note that the sharp double maximum can only be obtained for a clean probe compensated for stray circuit

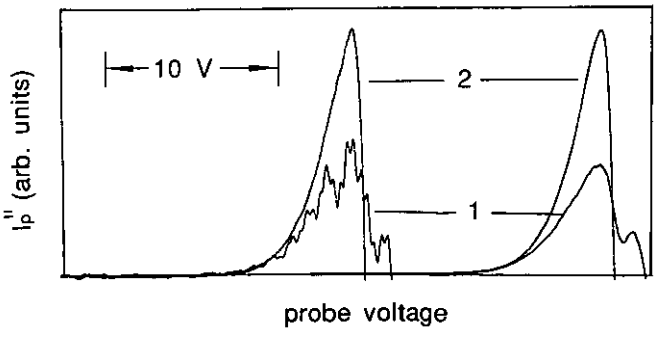

Figure 11. Second derivatives obtained in noisy DC discharge: 1, without noise suppression; 2, with noise suppression. Single traces are shown on the left side. Averaged traces are shown on the right.

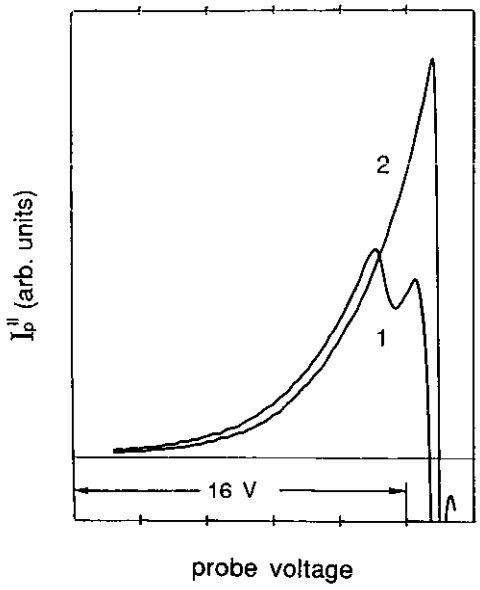

Figure 12. Second derivative obtained in He RF discharge of 13.56 MHz, $p = 0.1$ Torr, $V_d = 140$ V: 1, without filtering of the second harmonic; 2, with filtering.

resistance. Otherwise, only a broad maximum can be seen for a distorted $I_p''(V_p)$ with a large voltage interval between the maximum and the zero crossing (a typical case found in the literature for EEDF measurements in RF discharges).

4. Experimental results and discussion

4.1. Discharge conditions

EEDF measurements have been made in a radially confined, capacitive-coupled RF discharge symmetrically driven at 13.56 MHz. The EEDF measurements have been made together with accurate measurement of the RF discharge electrical characteristics [35, 37, 38] in a well defined discharge geometry. All probe measurements were performed in the midplane on the axis of an RF discharge located between two parallel-plate aluminium electrodes and radially confined by a Pyrex glass cylinder with a diameter of 14.3 cm and a corresponding discharge cross section $A = 160\,cm^2$. In some experiments the electrode separation L is 2 cm but the majority of measurements are done for $L = 6.7$ cm. The larger electrode separation makes it possible to maintain a discharge at considerably lower pressure and thus to study 'collisionless' RF discharges dominated by stochastic electron heating. Measurements were performed in argon and helium over a wide range of discharge conditions: gas pressure between 3 mTorr and 3 Torr, discharge current density between 0.1 and 10 mA cm^{-2}, discharge power flux between fractions and hundreds of mW cm^{-2} and discharge voltage between 20 and 1000 V. Over this wide range of discharge parameters, different ionization and electron heating mechanisms dominate in the formation of the EEDF, the fraction of discharge power

going into electron heating changes radically and the electron heating process itself changes from a local to non-local one [39].

For a fixed gas, electrode material, electrode gap and driving frequency, the discharge operational condition or mode can be characterized by gas pressure and discharge current density.

Starting from the lowest gas pressure at which an RF discharge with a given $L\omega$ is maintainable ($L/2 > S_0 \propto \omega^{-1}$, here S_0 is the averaged RF sheath width and ω is the driving frequency), one finds a so-called 'collisionless' regime for plasma electrons where stochastic electron heating in the oscillating RF sheaths at the plasma boundaries dominates and collisional (ohmic) heating in the bulk plasma due to electron–atom collision is small [39–44]. The collisionless regime is typically where the electron mean free path λ_e is comparable to or larger than the plasma half width $d = L/2 - S_0$. In a collisionless regime the electron energy relaxation length λ_ε is much larger than d and the EEDF is not in equilibrium with the local RF field. This situation is analogous to the limiting case of infinite electron thermal conductivity (grad $T_e \approx 0$) and is treated in the literature as a non-local regime in contrast to the opposite limiting regime of local equilibrium between the ionization frequency and the RF field [45, 46]. The EEDF in the non-local regime is a spatially homogeneous function of the total (kinetic + potential) electron energy $\varepsilon' = \varepsilon + e\phi$, where ϕ is the DC ambipolar potential [45]. A qualitative diagram of ion density n_i and the time-averaged electron density $\bar{n}_e$ distributions together with the ambipolar potential distribution are shown in figure 13 for a low-pressure RF discharge. In the plasma region where $n_i = n_e$ these distributions are similar to those given by the Tonks–Langmuir model [47], but they are considerably different in the RF sheath region ($n_e \ll n_i$) where a much larger DC voltage occurs due to the RF field rectification.

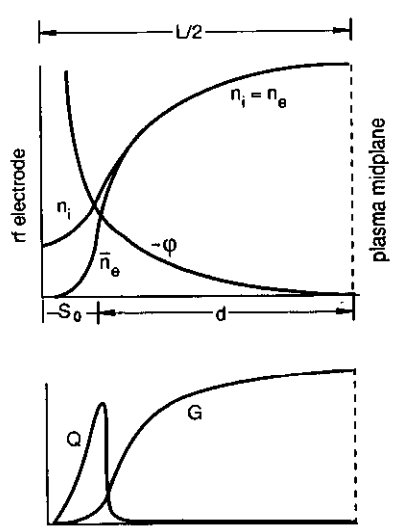

Figure 13. Axial distribution of ion density n_i, time averaged electron density n_e, ambipolar potential ϕ, ionization rate G and RF power density Q for electron heating in an RF discharge at the lowest gas pressure (non-local regime).

For a typical capacitively coupled RF discharge where the plasma frequency is much larger than the driving frequency, in the bulk plasma the RF field distribution $E_p(x)$ is inversely proportional to the plasma distribution $n(x) = n_i = n_e$, such that $E_p(x) \propto n^{-1}(x)$. This results in an inhomogeneous RF field (rising at the plasma boundary), and hence leads to an inhomogeneous rate of collisional electron heating $nE_p^2 \propto n^{-1}(x)$. However, at low gas pressures, the main electron heating near the plasma boundaries occurs via stochastic electron heating in the RF sheath [42, 52, 53]. Figure 13 qualitatively represents the spatial distribution of the electron heating rate as it was found in RF discharge simulations [49]. Also shown in figure 13 is the ionization rate distribution, which is nearly proportional to the electron density distribution, as expected for a rather homogeneous EEDF with the ionization frequency z being nearly constant along the discharge axis. Qualitatively, a different picture emerges for the opposite limiting case when the gas pressure is high and $\lambda_\varepsilon \ll d$ and the plasma electrons are in local equilibrium with the heating electric field. Under such conditions, electron and ion motion in the plasma body are collisionally dominated with the plasma spatial distribution controlled by ambipolar diffusion and collisional electron heating is the main RF power dissipation process. Due to local coupling between the EEDF and the RF electric field, the ionization frequency is space dependent resulting in a specific axial plasma density distribution [50, 51] which is rather homogeneous over most of the plasma with a sharp fall within the plasma boundaries as shown in figure 14. Since ionization and excitation frequencies are sharp functions of the RF field and $E \propto n^{-1}$, both the ionization rate and the plasma luminosity peak within the plasma boundaries, as qualitatively shown in figure 14. The two limiting cases described above occur in the present experiment at the lowest (few m Torr) and the largest (few Torr) gas pressures for relatively low discharge current when γ processes in the RF sheaths are negligible. In the intermediate range of gas pressure a hybrid RF discharge forms, bearing features of collisional and stochastic

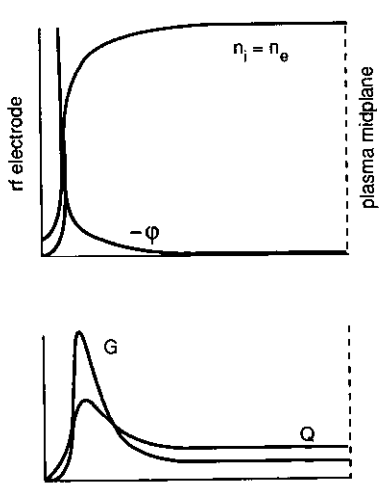

Figure 14. Axial distribution of the plasma parameters (given in figure 13) at high gas pressure (local regime).

electron heating and which can hardly be characterized as purely local or non-local.

With increasing discharge current (voltage and power) the RF discharge transits (smoothly of abruptly) to the γ mode [10] with a highly non-local (even at high pressures) plasma electron heating process. In the γ mode, secondary electrons (born at the RF electrode due to ion bombardment) and other electrons (due to electron avalanche or ion-ionization in the sheaths) accelerate in the RF sheaths towards the plasma where they perform intensive ionization and excitation. In the γ mode, the physical processes occurring in the RF sheaths and the bulk plasma are very similar to those that occur in the cathode sheath and the negative glow of a DC glow discharge. The rise of the discharge current (whether or not the discharge is in the γ mode) also increases the share of RF power going to ion acceleration in the sheaths. Therefore, at the high discharge current (voltage and power) only a negligible part of the total discharge power may be transferred to the electrons [33].

In that which follows, a brief overview of results recently obtained at GTE Laboratories is given. Some of these results were reported in conferences and are highlighted in [9, 54]. Detailed results on probe measurements of the plasma parameters and their relations to the electrical characteristics of RF discharges will be published in forthcoming papers.

4.2. EEDF in argon RF discharges at low pressure

Typical curves of the measured EEPF (electron energy probability function) and the corresponding EEDF are shown in figure 10 for the benchmark argon pressure $p = 0.1$ Torr in a discharge with $L = 2$ cm and a discharge current density $J = 2.65\,\mathrm{mA\,cm^{-2}}$. The striking result of these measurements is a significantly lower mean electron energy $\langle\varepsilon\rangle = 0.89\,\mathrm{eV}$ than that found in probe measurements carried out recently in argon RF discharges driven at 13.56 MHz at similar pL parameters [15, 19–21, 55]. The EEDF in figure 10 differs from a Maxwellian with $\langle\varepsilon\rangle = 0.89\,\mathrm{eV}$ and a corresponding effective electron temperature $T_{e\,\mathrm{eff}} = 0.59$ V in that it contains excessive numbers of fast and slow electrons. The EEPF in figure 10 can be represented as a sum of two Maxwellian distributions with two electron temperatures: $T_1 = 0.34$ V and $T_2 \approx 3.1$ V and corresponding electron densities of $n_1 = 1.32 \times 10^{10}\,\mathrm{cm^{-3}}$ and $n_2 = 1.3 \times 10^{9}\,\mathrm{cm^{-3}}$. The two-temperature feature of the EEPF at low argon pressure remains unchanged over a large range of discharge current density as shown in figure 15 where the EEPF is shown for J between 0.26 and $4.4\,\mathrm{mA\,cm^{-2}}$ and $p = 0.1$ Torr. Over the range of current density T_2 remains the same, while T_1 changes with rising J from 0.23 V to 0.39 V. The change in T_1 can be explained by the effect of electron–electron collisions which equalize the temperatures of the two electron groups and whose importance grows with increasing plasma density.

As shown in [9], the existence of two electron groups in the low-pressure argon RF discharge results from stochastic electron heating in the RF sheaths enhanced by

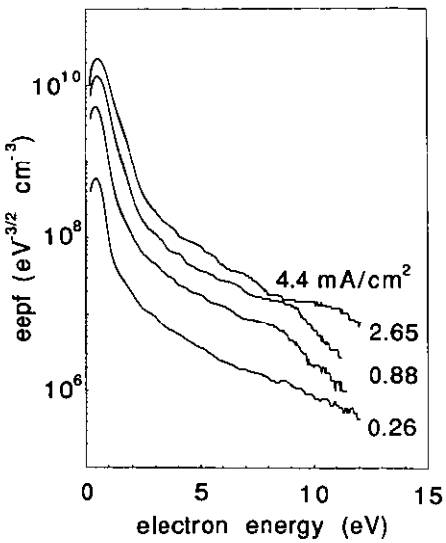

Figure 15. EEPF in an argon RF discharge for different discharge current densities with $L = 2$ cm and $p = 0.1$ Torr. $p = 0.1$ Torr.

the Ramsaur effect. Due to great temperature differences and the large Ramsauer effect in argon these two electron groups have essentially different properties and play significantly different roles in the RF discharge.

The low-energy group with its temperature close to the energy of the Ramsauer minimum ($\varepsilon_m \approx 0.3\,\mathrm{eV}$) has an extremely low electron–atom collision frequency ν_{en1} and $\lambda_{e1} \gg d = 0.6$ cm. The slow electrons are well Maxwellianized due to the large electron–electron collision frequency $\nu_{ee} \propto n T_e^{-3/2}$ and the reduced RF field in the plasma bulk [43]. Being trapped in the ambipolar potential well, the slow electrons oscillate collisionlessly in the weak RF plasma field (since $\nu_{en1}^2 \ll \omega^2$) unable to gain energy either from the RF field or from the oscillating RF sheaths which are accessible only to fast electrons [9].

The high-energy electron group, having a large ν_{en2} ($\nu_{en2}^2 \gg \omega^2$) and $\langle\varepsilon\rangle$, effectively interacts with argon atoms in elastic and ionization collisions and compensates their energy losses through stochastic heating on the oscillating plasma–sheath interfaces. Unlike low-energy electrons, the high-energy electrons easily overcome the ambipolar potential barrier and collide more frequently (than the slow electrons) with the axial plasma boundaries.

4.3. Heating mode transitions

Figure 16 demonstrates the evolution of the EEPF as the argon pressure is changed from 0.07 to 3.0 Torr at a fixed discharge current density of $2.65\,\mathrm{mA\,cm^{-2}}$ and for $L = 2$ cm [9]. At $L = 2$ cm the range of gas pressures was limited by discharge stability (prior to extinction) near 50 m Torr where the RF sheaths from the two electrodes nearly overlap, and by probe technique validity at the upper pressure. As seen in figure 16, EEPFs vary considerably in shape, being convex at high pressures and concave at low pressures and rapidly changing from one to the other at a threshold pressure $p_0 \approx 0.35$ Torr. This

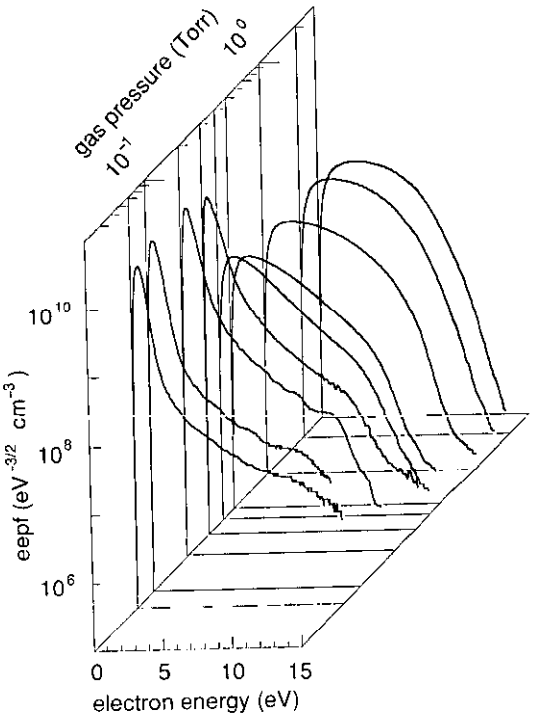

Figure 16. EEPF evolution with pressure in argon, $L = 2$ cm, $J = 2.65$ mA cm^{-2} [9].

transition is accompanied by a sharp change in the plasma density and mean electron energy, as is shown in figure 17. For pressure $p > 0.5$ Torr, the EEPFs are Druyvesteyn-like with $\partial f/\partial\varepsilon \to 0$ as $\varepsilon \to 0$; these are typical for an argon plasma in a DC or low-frequency field ($\nu_{en}^2 \gg \omega^2$) with no electron–electron interaction. The flattening of the EEPF as $\varepsilon \to 0$ is a consequence of the Ramsauer effect, when $\partial\nu_{en}/\partial\varepsilon > 0$ and low-energy electrons accelerate freely (without collision), thereby escaping the low-energy region of the EEDF. An opposite picture (the peaking of EEPF at small energy) takes place at $\nu_{en}^2 \ll \omega^2$ when the low-energy electrons oscillate without collisions. Consequently they gain no energy, and thus remain in the low-energy group. In the high-pressure, or collisional heating mode ($p > 0.5$ Torr), ohmic heating is the main RF power dissipation process [9]. As the gas pressure decreases, stochastic heating quickly becomes the dominant electron heating process. As a consequence of the non-local character of the RF discharge energy balance at these low pressures [41, 43], the addition of stochastic heating at the oscillating boundaries leads to a reduction in the bulk RF field. This reduces the electron energy, and since in argon $\nu_{en} \propto \varepsilon^{3/2}$, it reduces the collisional bulk electron heating even more. This kind of positive feedback provides an abrupt transition when the discharge changes from a collisional to a stochastic heating mode as the gas pressure goes down. As shown in [9], the threshold pressure p_0 corresponds to a $p_0 d$ product where collisional and stochastic heating is nearly equal (as is seen in figure 17). Measurements in an argon RF discharge with $L = 6.7$ cm and $J = 3$ mA cm^{-2} (shown in figure 18) demonstrate a similar evolution of the EEPF with gas pressure, but the transition occurs at a lower gas pressure ($p_0 = 70$ mTorr) such that the product $p_0 d$ is very close to that for $L = 2$ cm. This, it seems, confirms the scaling law for heating mode trans-

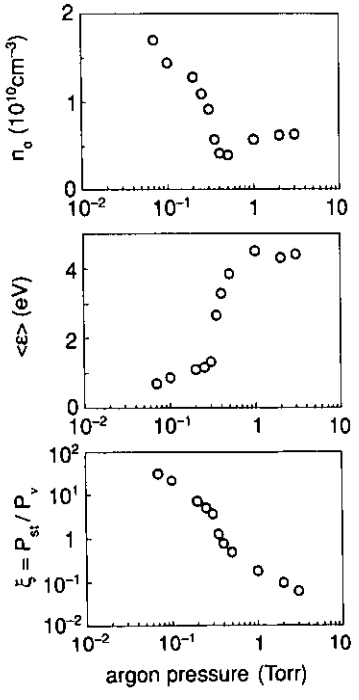

Figure 17. Plasma density n_0, mean electron energy $\langle\varepsilon\rangle$ and ratio of stochastic to collisional power ξ versus argon pressure. $L = 2$ cm, $J = 2.65$ mA cm^{-2} [9].

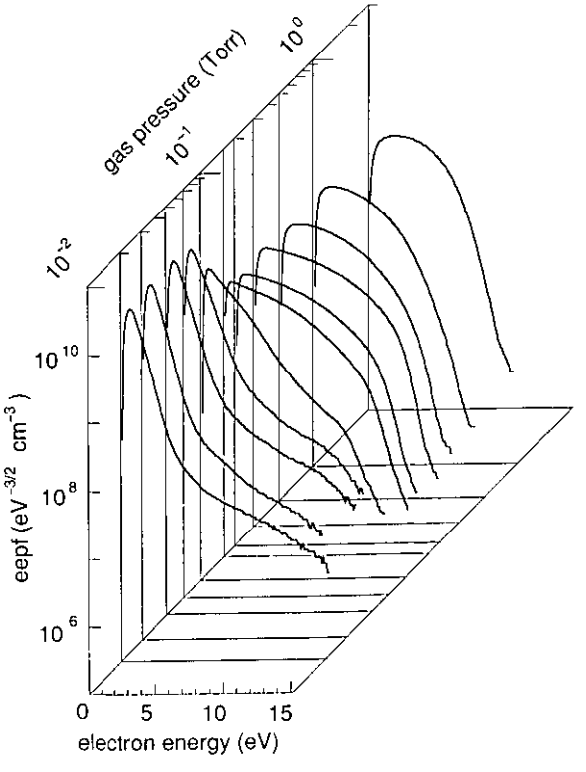

Figure 18. EEPF evolution with pressure in argon. $L = 6.7$ cm, $J = 3$ mA cm^{-2}.

itions found in [9] in argon RF discharges at 13.56 MHz: $p_0 d \approx 0.2$ Torr cm.

The effective electron temperature $T_{eff} = 2/3\langle\varepsilon\rangle$ has different trends for collisional and stochastic modes. Thus, for discharges with $L = 2$ cm and $L = 6.7$ cm, T_{eeff} in collision-dominated discharges (large pL) decreases slightly with increasing pL and discharge current (as is common in gas discharge plasmas). Quite oppositely, for the stochastic heating mode, the temperature T_{e1} of the low-energy group, accounting for 90% of all electrons, grows slightly with increasing pL and discharge current, while the temperature T_{e2} of the high-energy group remains nearly constant. The increase in T_{e1} with growth in the discharge current can be explained as the effect of e–e collisions between the two electron groups and whose importance grows with increasing plasma density. Increases in T_{e1} with gas pressure may also be the result of additional collisional heating.

Having measured the EEDF, the plasma density and the discharge current, one can estimate (from plasma conductivity) the collisional power deposition P_{col} and compare it with the total RF power transferred to the plasma electrons P_{meas}. The latter term can be found from the measured power versus current characteristic, subtracting the ion acceleration power in the RF sheaths [33]. The ratio P_{meas}/P_{col} found in this way is shown in figure 19 for argon discharges with $L = 6.7$ cm and $J = 1$ mA cm^{-2}. This ratio starts to differ considerably from unity at the same argon pressure at which the EEPF begins to change shape (see figure 20). At low pressure P_{meas}/P_{col} reaches 10^3, evidently demonstrating the effect of non-collisional stochastic electron heating.

A comparison of EEPFs measured in argon and helium RF discharges under similar conditions ($L = 6.7$ cm, $J = 1$ mA cm^{-2}) is shown in figures 20 and 21. In contrast with argon, no peak in $f(\varepsilon)$ is found at low energies in helium discharges. Over all gas pressures in helium, most electrons in the body of the EEPF have a Maxwellian

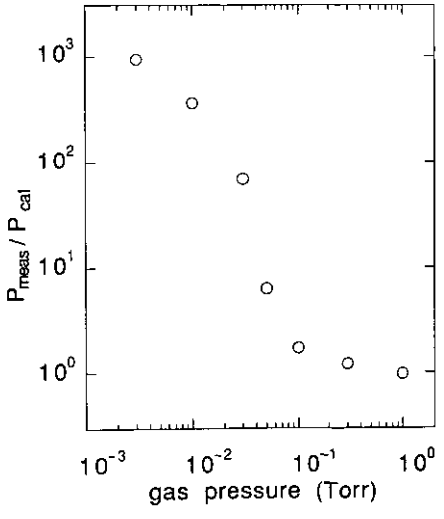

Figure 19. The ratio between total and collisional RF power transferred to the plasma electron versus argon pressure. $L = 6.7$ cm, $J = 1$ mA cm^{-2}.

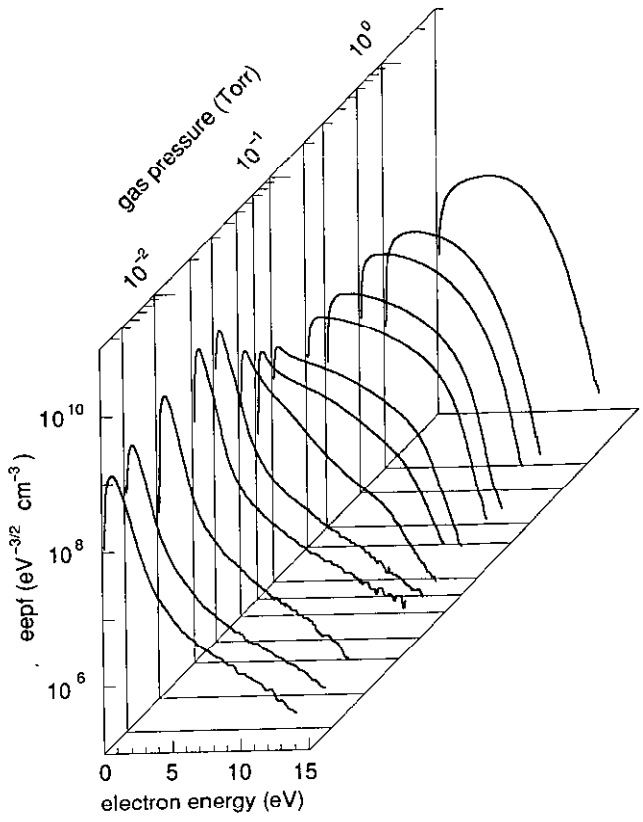

Figure 20. EEPF evolution with pressure in argon. $L = 6.7$ cm, $J = 1$ mA cm^{-2}.

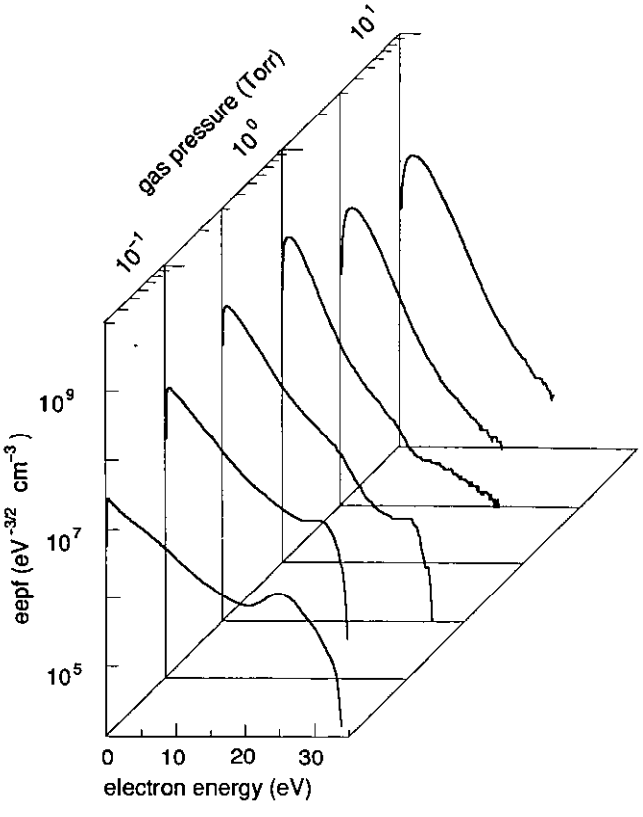

Figure 21. EEPF evolution with pressure in helium. $L = 6.7$ cm, $J = 1$ mA cm^{-2}.

distribution with T_{eeff} falling as the gas pressure grows (similar EEPF behaviour in a helium RF discharge was found in [17]), while in argon an abnormal behaviour for T_{eeff} is observed as shown in figure 22 at $L = 6.7$ cm and $J = 1\,\text{mA cm}^{-2}$ (for both gases). Thus, the comparison of the EEPF shapes and dependence of T_{eeff} on pressure for argon and helium RF discharges seems to confirm that the abnormal low electron energy and sharp heating mode transition is intrinsic to a Ramsauer gas.

The decisive role of the Ramsauer effect on the shape of the EEPF in RF discharges has been demonstrated recently through particle simulation of a helium RF discharge with an artificially introduced Ramsauer-like electron–atom cross section [56]. Nonetheless, it is possible that a low-temperature electron group may develop in a non-Ramsauer gas like helium, occurring at a much greater ω/pd than in the present experiments. Our calculation (similar to those shown in figure 19) for a helium RF discharge at $L = 6.7$ and at the minimal maintainable gas pressure $p_{min} = 30$ mTorr showed that the stochastic heating is comparable to or just a little larger than collisional (ohmic) heating.

Another kind of RF discharge mode transition is shown in figure 23 where the EEPF evolution with gas pressure is given for a helium RF discharge at $J = 3\,\text{mA cm}^{-2}$. At a fixed discharge current density, the RF discharge voltage V_d is a falling function of gas pressure p, and at some intermediate pressure, between 0.3 and 1 Torr in figure 23, an appropriate combination of pS_0 and V_d occurs for an electron avalanche to develop in the RF sheaths leading to a transition of the discharge into the γ mode. The functionality of $pS_0(V_d)$ corresponding to this transition is similar to a Paschen breakdown curve. EEPFs in the γ mode ($p = 0.3$ and 1 Torr) demonstrate a Maxwellian distribution with extremely low electron temperatures over a dynamic range of three to four orders of magnitude. At lower gas pressures, there are not enough electron–atom collisions in the RF sheaths for an electron avalanche to develop there, and the EEDF is little affected by the secondary electrons produced by ion bombardment of the RF electrodes. Only

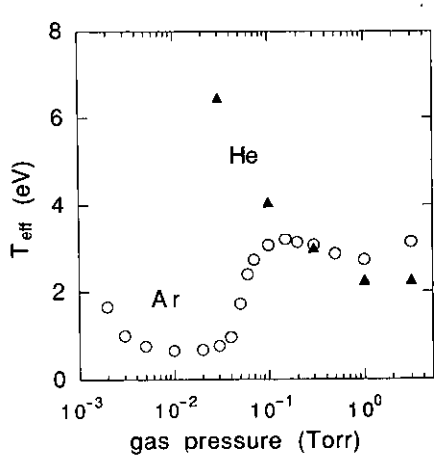

Figure 22. Effective electron temperature in argon and helium RF discharges. $L = 6.7$ cm, $J = 1\,\text{mA cm}^{-2}$.

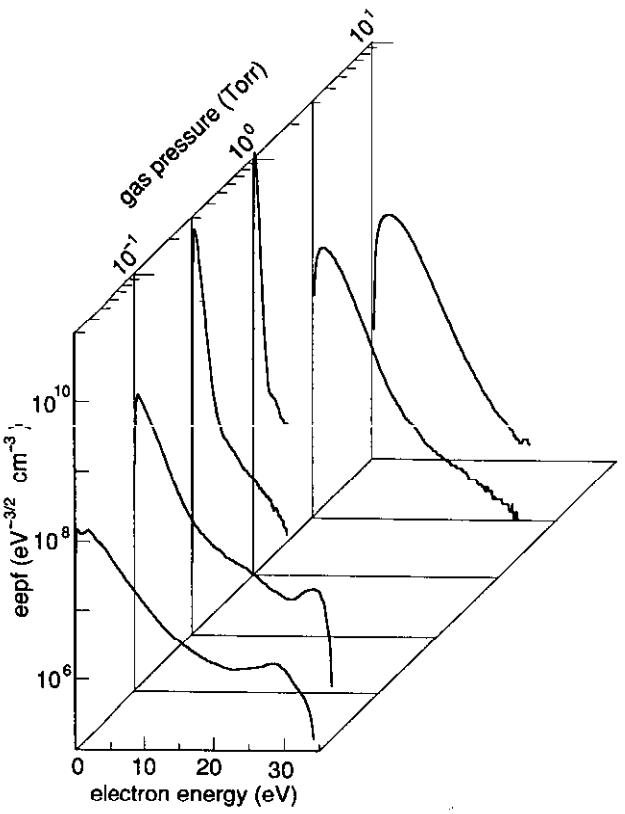

Figure 23. EEPF evolution with pressure in helium. $L = 6.7$ cm, $J = 3\,\text{mA cm}^{-2}$.

at very high RF voltages ($V_d \geqslant 1$ kV) can secondary electrons and the electrons generated in the RF sheaths due to ionization produced by the high-energy ions [57] affect the EEDF in the plasma body. For a large gas pressure (3 and 10 Torr in figure 23) at $J = 3\,\text{mA cm}^{-2}$ the RF voltage in the sheaths is too small to maintain an electron avalanche, and thus to initiate an RF discharge transition to the γ mode. EEDFs in the γ mode are considered in section 4.5.

Two different kinds of distortion in the measured low-energy part of the EEPF (actually, the second derivative of the probe characteristic) are observed in figure 23 for extremely low and high gas pressures. The first one at 30 mTorr apparently is RF distortion due to an extremely large discharge voltage (see equation (5)) and a small n_0/T_e ratio making the probe plasma capacitance smaller than about 10 pF measured in argon discharge where n_0/T_e is much larger than in helium. The other kind of distortion at 3 Torr and especially at 10 Torr is due to high gas pressure where λ_e becomes comparable to or even smaller than the probe radius a. In both kinds of distortion (RF and 'large probe'), the exponential extrapolation technique mentioned in section 3.5 has been used to calculate T_{eeff} and n_0. It seems that this extrapolation is only a reasonable remedy for weakly distorted second derivatives. For 10 Torr, a real deconvolution technique [58, 59] or a collisional probe theory (see [60] and literature cited therein) is needed to interpret the EEPF from probe measurements.

4.4. Super-thermal electrons and electron beams

EEPFs measured in argon at low pressure and in helium at all pressures demonstrate an excessive number of high-energy electrons, i.e. more than that expected for a Maxwellian EEDF. These electrons, called super-thermal electrons, are due to stochastic electron heating in the RF sheaths, collisional overheating in the strong RF fields near the plasma boundaries, secondary-electron emission at the electrodes and electron avalanche (at higher pressure) and/or ion ionization [57] (at lower pressure) in the RF sheaths. The contribution of each of these processes depends on the specific discharge conditions governed by the discharge's external parameters: p, L, ω and J.

In any case, the excess of high-energy electrons in a weakly ionized plasma generally results in cooling of the main body of electrons, thus reducing the effective electron temperature. This paradoxical effect of electron cooling by introduction of hot electrons is a consequence of the ionization balance of bounded non-equilibrium plasmas. A pronounced and well known example of such a cooling is the extremely low electron temperature found in the cathode glow region of a DC glow or low-pressure arc discharge. Similar phenomena take place in RF discharge in the γ mode.

At the lowest gas pressure in argon where the RF discharge is controlled by stochastic heating, the electron cooling effect is most explicitly demonstrated as an abnormally low effective electron temperature, but electron cooling should also occur to some extent in non-Ramsauer gases and also for collisional electron heating localized at the plasma boundaries. Indeed, the electron temperatures in helium RF discharge found from our measurements seem to be smaller than those typically found in the literature for the positive column of helium DC discharges with a $pR \approx pd$, where R is the positive column radius.

EEPFs measured in helium at low pressures (figures 21, 23) have peculiar 'bumps' on $f(\varepsilon)$ near $\varepsilon \approx 25\,\mathrm{eV}$, followed by a zero crossing. This is shown for helium on a linear scale in figure 24(*a*). Similar behaviour was found for argon (figure 24(*b*)) after making a special effort to increase the dynamic resolution of the measurement. The bumps and negative values of I'' were found to disappear as the gas pressure grew, as shown in figure 24(*c*) for a helium RF discharge with $L = 6.7\,\mathrm{cm}$ and $J = 1\,\mathrm{mA\,cm^{-2}}$.

The negative values for I'' signify a high degree of anisotropy in the EEDF where the Druyvesteyn formula is not valid [61–63]. Therefore, the measured EEPFs for energies of about 25–30 eV should be only considered as qualitative. Note also, that the dynamic range of the EEPF measurements is limited by the masking effect of the second derivative of the ion probe current, especially for light gases like helium. Nonetheless, the bumps and negative values of I'' point out a directed electron beam having energy considerably higher (especially in argon) than the mean electron energy. Recently, a high degree of electron anisotropy in a low-pressure argon RF discharge

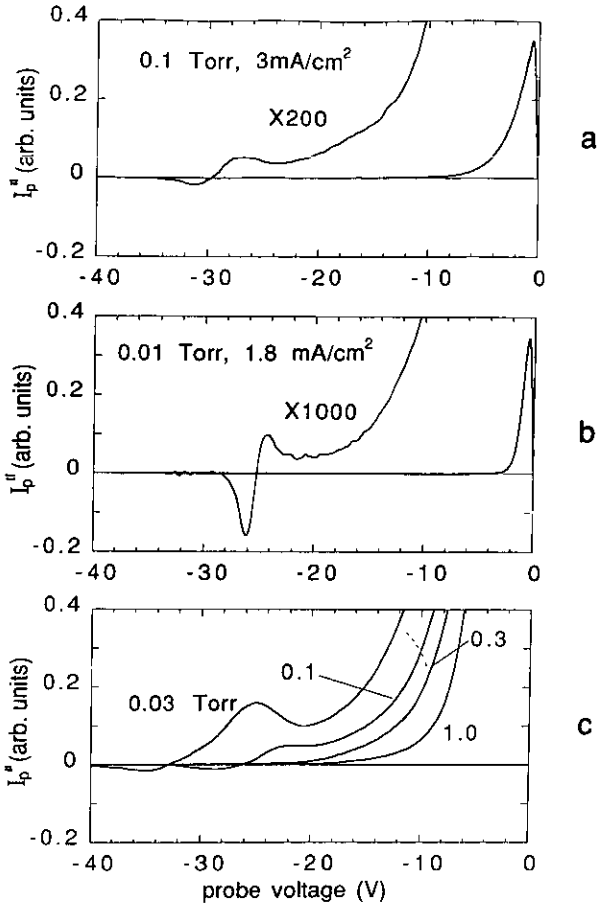

Figure 24. Second derivatives in anisotropic RF plasma. $L = 6.7\,\mathrm{cm}$.

was demonstrated in measurements with a single-sided flat probe [64]. It is believed that the existence of directed electron beams in low-pressure RF discharges was first found using polarization spectroscopy [65, 66]. Recent experiments with spatial–temporal-resolved emission spectroscopy [67] and particle simulation experiments [49, 68, 69] also show the existence of super-thermal directed electron beams in low-pressure RF discharges.

The directed high-energy electrons are accelerated during reflection from the moving plasma–RF sheath interfaces at the moment of maximum sheath velocity. As follows from emission spectroscopy and particle simulations, the ballistic electrons cause ionization and excitation waves propagating along the RF discharge. It is interesting to note that in particle simulation experiments [69] carried out for an argon RF discharge ($\omega/2\pi = 13.56\,\mathrm{MHz}$, $L = 10\,\mathrm{cm}$ and $p = 3\,\mathrm{mTorr}$) the maximum in the anisotropic electron velocity distribution was found at $v_e \approx 4 \times 10^8\,\mathrm{cm\,s^{-1}}$, which is very close to that in our experiments: $v_e = 3 \times 10^8\,\mathrm{cm\,s^{-1}}$.

Some excess of high-energy electrons seen in helium RF discharges at relatively high pressures of 1–5 Torr may result from the collisional overheating in the vicinity of the plasma boundaries as well as from super-elastic collisions of thermal electrons with metastable excited helium atoms and Penning ionization processes with

participation of two excited helium atoms. Such phenomena were demonstrated for helium and argon plasmas by direct measurement of the EEDF in the after-glow stage where in absence of the heating electric field the super-elastic collisions and Penning ionization were the only sources of high-energy electrons [70]. Note that the mid-plane region of a parallel-plate RF discharge with ionization, excitation and electron heating processes localized at the plasma axial boundaries and with some reduced RF field in the midplane can be thought of as a 'spatial afterglow'. Again, due to the masking effect on the second derivative of the ion current at high electron energies, any speculation about the actual behaviour of the EEPF in helium found in the present work for a dynamic range of more than three or four orders of magnitude is questionable.

4.5. EEDF in the γ mode

Having a probe measurement system with improved energy resolution we were able to demonstrate, for the first time, the EEDF evolution during the RF discharge transition into the γ mode [54]. Figure 25 shows the evolution of the EEPF with discharge current density in argon RF discharges ($L = 6.7$ cm and $p = 0.3$ Torr). Corresponding integrals of the EEDF, the plasma density n_0 and the effective electron temperature T_{eeff}, together with corresponding discharge parameters, voltage and power density, are shown in figure 26. The same diagrams for RF discharges under similar conditions in helium are shown in figures 27 and 28. Figures 25 and 27 show that at relatively small currents the EEPF in argon resembles a Druyvesteyn distribution while in helium it is more like a Maxwellian. Over a limited range of increasing discharge current, the EEPF does not change shape appreciably, T_{eeff} remains fairly constant and the plasma density grows linearly. The differences in the EEPFs for both gases in the energy interval below the inelastic threshold energy (11.6 eV for argon and 19.8 eV for helium) are due to differences in the functionality of the elastic electron–neutral collision frequency $\nu_{en}(\varepsilon)$ for argon and helium [71, 72].

Further increases in the discharge current, however, lead to an abrupt change in the EEPF shape with a corresponding drop in the T_{eeff} and a rapid increase in plasma density. For both gases, the EEPFs become Maxwellian over a large dynamic range (three orders of magnitude). This is a consequence of a sharp increase in electron–electron collision frequency, $\nu_{ee} \propto n_0/T_e^{3/2}$ together with the reduced plasma RF field, $E_0 \propto J/n_0$ [54].

The transition point where the discharge switches from the α mode to the γ mode, defined as the steepest part of the $T_{eeff}(J)$ dependence, corresponds to a transition current density J_{tr} and a transition voltage V_{tr} of 5 mA cm^{-2} and 200 V for argon and 2 mA cm^{-2} and 180 V for helium, respectively. These transition voltages are comparable to the normal cathode fall voltage in a DC glow discharges. For both gases V_{tr} correlates well

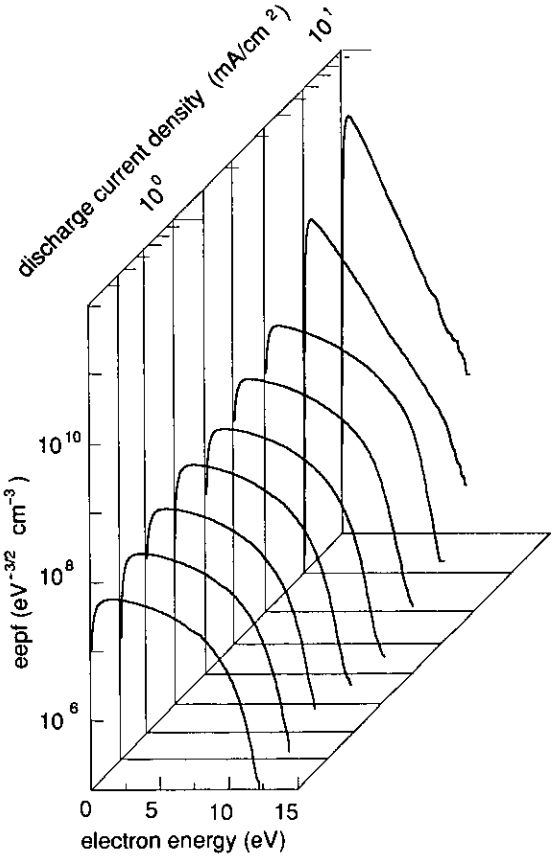

Figure 25. EEPF evolution during RF discharge transition to the γ mode. $L = 6.7$ cm; argon at $p = 0.3$ Torr [54].

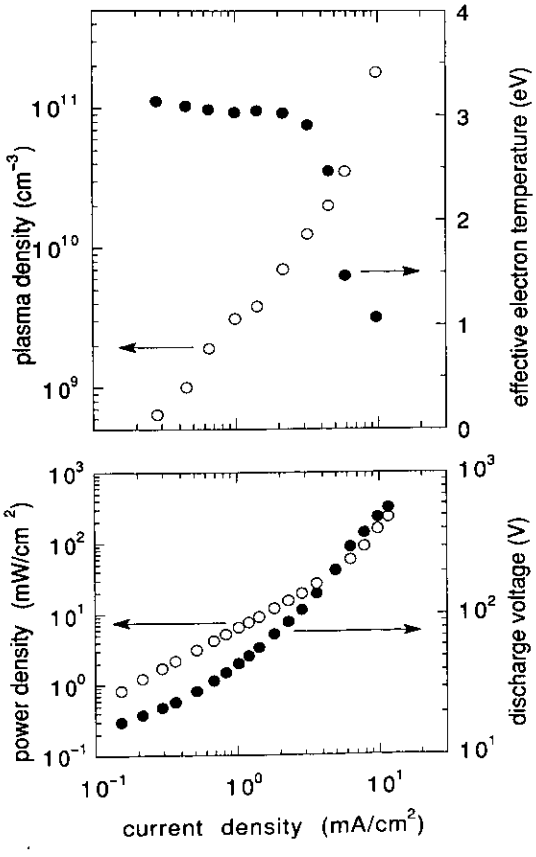

Figure 26. Discharge and plasma parameters for argon RF discharge [54].

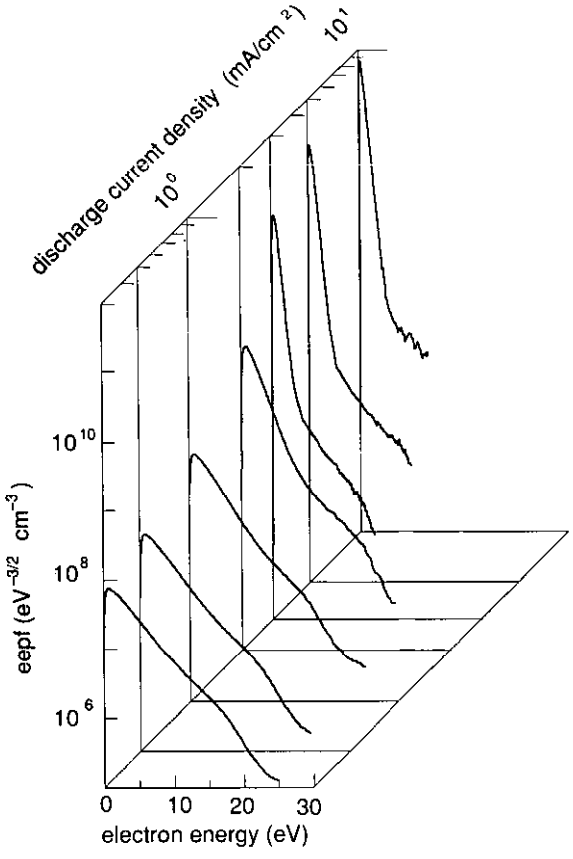

Figure 27. EEPF evolution during RF discharge transition to the γ mode. $L = 6.7$ cm; helium at $p = 0.3$ Torr [54].

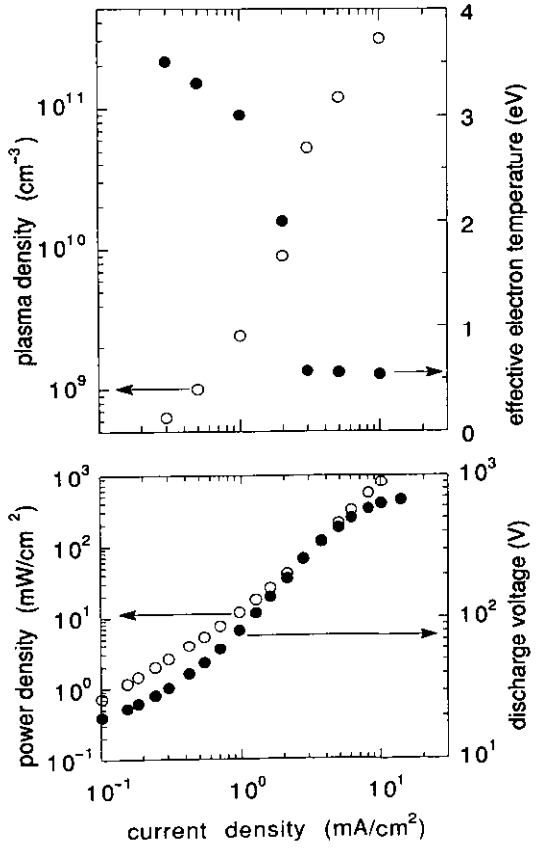

Figure 28. Discharge and plasma parameters for helium RF discharge [54].

with a change in the discharge colour (luminosity) observed in experiment. However, as one can see in figure 28 for helium, the departure from linear current/voltage characteristic (which further leads to the discharge voltage saturation) takes place somewhere between 400 and 500 V which is more than twice the V_{tr} found from the $T_{eeff}(J)$ dependence. No trend in the discharge voltage saturation is seen in argon, although changes in the EEPF and in the discharge luminosity were evident.

The abrupt changes in the EEPF and in the plasma parameters are well known in RF discharge literature as the transition into the γ regime. In the γ regime ion bombardment initiates secondary-electron emission from the RF electrodes; electron acceleration and multiplication in the large electric fields within the RF sheaths produce intensive ionization in the plasma body, accompanied by a sharp growth in plasma density and a drop in electron temperature.

The transition into the γ regime and the corresponding plasma parameter behaviour shown here is very similar to that first found in helium RF discharges at 3.2 MHz and described in an analytical hydrodynamic model of an RF discharge in the γ mode based on the assumption of two electron groups [10]. The electron kinetics in the bulk plasma of the γ mode is similar to that in the cathode glow of a DC glow discharge, since in both cases ionization is maintained by a swarm of hot electrons generated in the cathode (RF electrode) sheath while the electric field in the plasma is significantly lower than that in a self-sustaining plasma.

It was not possible to analyse the high-energy γ electrons which presumably perform ionization and gas excitation. Having an energy comparable to the RF sheath voltage, the γ electrons accelerated in the RF sheaths have a high ionization efficiency and thus the ionization balance of an RF discharge in the γ mode requires only an extremely small number of γ electrons [10]. The limited dynamic resolution (about four orders of magnitude) in the second-derivative measurement and the masking effect of the ion current make detection of γ electrons with probe techniques highly problematic.

The electron temperature of the main body of electrons measured in a well developed γ mode (at $J = 10\,\mathrm{mA\,cm^{-2}}$, $L = 6.7$ cm), when T_e reaches its minimum value T_{emin}, are shown in figure 29 as a function of the helium gas pressure. The fall in the electron temperature with increasing gas pressure is a consequence of the change in the electron energy balance mainly due to a drop in the electron heating power [54].

In the γ mode developed at relatively high gas pressure, the swarm of fast γ electrons generated in the RF sheaths quickly decays in the plasma, providing ionization only near the plasma boundaries. From there, the cold electrons produced by the γ electrons diffuse to the plasma centre and vanish due to radial diffusion and/or recombination. The last process is very probable due to the extremely low electron energy [73–75]. The picture described here is equivalent to that in the Faraday dark space of a DC glow discharge.

The electron temperature of 52 mV (or 600 K) meas-

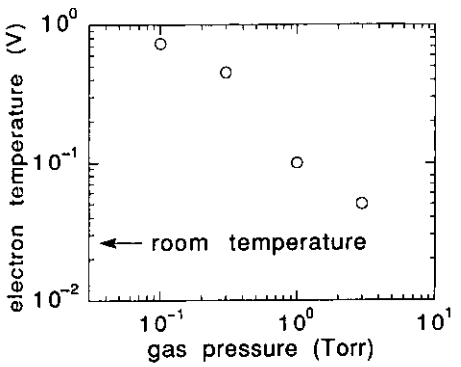

Figure 29. Electron temperature in a well developed γ mode. $L = 6.7$ cm, $J = 10\,\mathrm{mA\,cm^{-2}}$ [54].

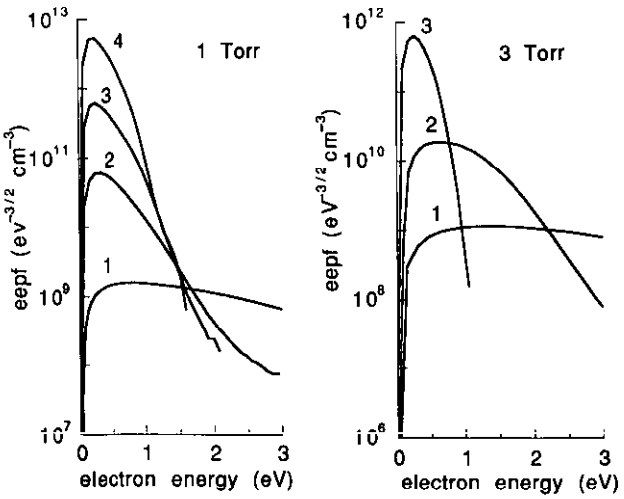

Figure 30. EEPF (second derivative) evolution during helium rf discharge transition to the γ mode. $L = 6.7$ cm. For $p = 1$ Torr (left-hand diagram): (1) $J = 2\,\mathrm{mA\,cm^{-2}}$; (2) $J = 3\,\mathrm{mA\,cm^{-2}}$; (3) $J = 5\,\mathrm{mA\,cm^{-2}}$; (4) $J = 10\,\mathrm{mA\,cm^{-2}}$. For $p = 3$ Torr (right-hand diagram): (1) $J = 4$ mA cm^{-2}; (2) $J = 5.5$ mA cm^{-2}; (3) $J = 10$ mA cm^{-2}.

ured in a helium RF discharge at 3 Torr is close to that typically found in the negative glow of a DC discharge (see [76] and literature cited therein) and it is close to the radiation temperature in a helium RF discharge ($p = 0.5$ Torr, $f = 2.5$ MHz) found from microwave diagnostics [77].

Our experience with EEDF measurements has shown that an RF discharge in the γ mode is the most demanding circumstance for probe diagnostics. The largest discharge voltage and the smallest electron temperature ($V_d/T_e < 10^3$), both of which are typically found in the γ mode, make it difficult to attain sufficient energy resolution in the measurement. At large discharge voltages, intensive probe contamination with sputtered RF electrode materials makes it impossible to perform meaningful probe measurements without continuous probe cleaning. An additional complication in the EEDF measurements in the γ mode is that T_e can be considerably less than the voltage gap between the maximum and the zero crossing of the second derivative $I_p''(V_p)$. This gap, which is due to inhomogeneity of the probe work function and, possibly, electron reflection of the probe surface and limited bandwidth of the probe circuitry, prevents the majority of electrons of the distribution with low electron temperature from being analysed. Such a situation is shown in figure 30 for EEPF evolution at the discharge transition to the γ mode corresponding to $p = 1$ and 3 Torr. Here, the smoothing of the second-derivative maximum is evident at the highest discharge currents. For these cases, the relatively large gap ΔV makes it meaningless to exponentially extrapolate the second derivative $I_p''(V)$ at the zero-crossing point, since it leads to an increase in $I_p''(V_p)$ by several orders of magnitude and to an exaggerated value of n_0. Fortunately, in these cases $I_p''(V_p)$ is an exponential function over two to three orders of magnitude. That, together with a strong case for a Maxwellian distribution (an extremely large n_0/T_e ratio), makes the evaluation of the electron temperature rather certain. The plasma density can then be easily found from probe I/V characteristics, which manifest well pronounced electron current saturation, since for such a dense and cold plasma even a small-radius probe works as a flat one ($\lambda_D \ll a$).

Note that the electron temperatures found here from EEDF measurements in the γ mode are significantly lower than those found in [10] using traditional Langmuir probe techniques. The main reason for this difference is essentially an improvement in the developed probe diagnostic system which allows us to address the variety of problems encountered in EEDF measurements in RF plasmas.

5. Conclusion

EEDF measurements in RF plasmas are a most difficult and challenging case in probe diagnostics requiring incorporation of a great deal of experience accumulated since Langmuir's time and special attention to many details in the design of the probe measurement system. Many of the problems in EEDF measurements in low-pressure RF-driven plasmas have been discussed and a probe measurement system specifically designed to avoid these problems has been described here in some detail. It should be pointed out that no new techniques have been introduced here that have not been considered elsewhere. However, this may be the first time that these techniques have been incorporated into one measurement device, resulting in significantly improved overall performance of the probe diagnostic system.

With this probe system a systematic experimental study of the EEDF has been carried out in capacitively coupled RF discharges in argon and helium over a wide range of gas pressures and discharge currents. The measurements readily show the specific changes in the EEDF that occur due to stochastic electron heating and discharge transition into the γ mode, as well as the substantial differences in the EEDF of Ramsauer and non-Ramsauer gases. For the first time, the evolution of the EEDF resulting from changes in the discharge-sustaining mechanisms has been demonstrated.

References

[1] Druyvesteyn M J 1930 *Z. Phys.* **64** 781
[2] Godyak V A 1990 Measuring EEDF in gas discharge plasmas (review) in *Plasma–Surface Interaction and Processing of Materials NATO Advanced Study Institutes, Ser. E, vol 176)* ed O Auciello *et al* (Dordrecht: Kluwer Academic) pp 95–134
[3] Schott L 1968 *Plasma Diagnostics* ed W Lochte-Holtgreven (Amsterdam: North Holland) ch 11
[4] Godyak V A 1988 Langmuir probe diagnostics in RF plasma (a critical review) *Report E-23, 41st Ann. GEC (Minneapolis, MN, October 1988);* 1986 *Soviet Radio Frequency Discharge Research* (Falls Church, VA; Delphic Associates) pp 118–38
[5] Waymouth J F 1964 *Phys. Fluids* **7** 1893; 1966 *Phys. Fluids* **9** 801
[6] Swift J D and Schwar M J R 1969 *Electrical Probes for Plasma Diagnostics* (New York: American Elsevier) pp 173–83
[7] Waymouth J F 1966 *J. Appl. Phys.* **37** 4493
[8] Waymouth J F 1989 Plasma diagnostics in electrical discharge light sources in *Plasma Diagnostics* vol 1 (New York: Academic) pp 47–111
[9] Godyak V A and Piejak R B 1990 *Phys. Rev. Lett.* **65** 996
[10] Godyak V A and Khanneh A S 1986 *IEEE Trans. Plasma Sci.* **14** 112
[11] Godyak V A and Popov O A 1977 *Sov. Phys.–Tech. Phys.* **22** 461
[12] Gagne R R J and Cantin A 1972 *J. Appl. Phys.* **43** 2639;
Cantin A and Gagne R R J 1977 *Appl. Phys. Lett.* **30** 316
[13] Godyak V A and Oks S N 1979 *Sov. Phys.–Tech. Phys.* **24** 1255
[14] Wiesemann K 1967 *Phys. Lett.* **25A** 701
[15] Cox T I, Deschmukh V G I, Hope D A, Hydes A J, Braithwaite N St J and Benjamin N M P 1987 *J. Phys. D: Appl. Phys.* **20** 820
[16] Sabadil H, Klagge S and Kammeyer H 1988 *Plasma Process. Plasma Chem.* **8** 425
[17] Dilecce G, Capitalli M and De Benedictis S 1991 *J. Appl. Phys.* **69** 121
[18] Godyak V A and Piejak R B 1990 *J. Appl. Phys.* **68** 3157
[19] Braithwaite N St J, Benjamin N M P and Allen J E 1987 *J. Phys. E: Sci. Instrum.* **20** 1046
[20] Wilson J L, Caughman J B O II, Phi Long Nguyen and Ruzic D N 1989 *J. Vac. Sci. Technol.* A **7** 972
[21] Paranjpe A P, McVittie J P and Self S A 1990 *J. Appl. Phys.* **67** 6718
[22] Chatterton P A, Rees J A, Wu W L and Al-Assadi K 1991 *Vacuum* **43** 489
[23] Kagan Yu M, Kolokolov N B, Lyagushenko R I, Milenin V M and Mirzabekov A M 1971 *Sov. Phys.–Tech. Phys.* **16** 561
[24] Matsumura S and Chen Sin-Li 1979 *Rev. Sci. Instrum.* **50** 1975
[25] Godyak V A, Lagushenko R I and Maya J 1988 *Phys. Rev. A* **38** 2044
[26] Laframboise J G 1966 *University of Toronto Institute for Aerospace Study Report* No 100
[27] Mosburg E R 1981 *Rev. Sci. Instrum.* **52** 1182
[28] Allen M W, Annaratone B M and Allen J E 1988 *Proc. 9th Int. Conf. on Gas Discharges and their Applications (Venice)* (Padova, Italy: Benetton Editore) p 487
[29] Jaeger E F, Berry L A and Batchelor D B 1991 *J. Appl. Phys.* **69** 6918
[30] Dovzhenko V A, Ershov A P and Solntsev G S 1974 *Sov. Phys.–Tech. Phys.* **19** 851
[31] Van den Hoek W G M, de Vries C A M and Heijman M G L 1987 *J. Vac. Sci. Technol.* B **5** 647
[32] Butterbaugh J W, Baston L D and Sawin H H 1990 *J. Vac. Sci. Technol.* A **8** 916
[33] Godyak V A, Piejak R B and Alexandrovich B M 1991 *J. Appl. Phys.* **69** 3455
[34] Godyak V A, Piejak R B and Alexandrovich B M 1990 *Rev. Sci. Instrum.* **61** 2401
[35] Godyak V A and Piejak R B 1990 *J. Vac. Sci. Technol.* A **8** 3833
[36] Horowitz P and Hill W 1981 *The Art of Electronics* (Cambridge University Press) p 151
[37] Godyak V A and Piejak R B 1990 *ESCAMPIG-90* ed V Debreuil (Orléans: European Physical Society) p 417
[38] Godyak V A, Piejak R B and Alexandrovich B M 1991 *IEEE Trans. Plasma Sci.* **19** 660
[39] Godyak V A 1986 *Soviet Radio Frequency Discharge Research* (Falls Church, VA: Delphic Associates)
[40] Godyak V A 1972 *Sov. Phys.–Tech. Phys.* **16** 1073
[41] Godyak V A 1976 *Sov. J. Plasma Phys.* **2** 78
[42] Popov O A and Godyak V A 1985 *J. Appl. Phys.* **57** 53
[43] Popov O A and Godyak V A 1986 *J. Appl. Phys.* **59** 1759
[44] Godyak V A and Popov O A 1979 *Sov. J. Plasma Phys.* **5** 227
[45] Tsendin L D 1979 *Sov. Phys.-JETP* **39** 805
[46] Feoktistov V H, Popov A M, Popovicheva O B, Rakhimov A T, Rakhimova T V and Volkova E A 1991 *IEEE Trans. Plasma Sci.* **19** 163
[47] Tonks L and Langmuir I 1929 *Phys. Rev.* **34** 876
[48] Godyak V A 1986 *Soviet Radio Frequency Discharge Research* (Falls Church, VA: Delphic Associates) p 80
[49] Surendra M and Graves D B 1991 *IEEE Trans. Plasma Sci.* **19** 144
[50] Godyak V A and Hanna A H 1979 *Sov. J. Plasma. Phys.* **5** 376
[51] Godyak V A and Hanna A H 1980 *Sov. J. Plasma Phys.* **6** 372
[52] Goedde C G, Lichtenberg A J and Liebermann M A 1988 *J. Appl. Phys.* **63** 4375
[53] Lieberman M A 1988 *IEEE Trans. Plasma Sci.* **16** 638
[54] Godyak V A, Piejak R B and Alexandrovich B M 1992 *Phys. Rev. Lett.* **68** 40
[55] Terai K J, Kaneda T and Chang J S 1989 *42nd Annual GEC (Palo Alto, CA)* report J-5 (Menlo Park, CA: SRI International)
[56] Surendra M and Graves D B 1991 *Phys. Rev. Lett.* **66** 1469
[57] Trombley H W, Terry F L Jr and Elta M E 1991 *IEEE Trans. Plasma Sci.* **19** 158
[58] Swift J D and Schwar M J R 1969 *Electrical Probes for Plasma Diagnostics* (New York: American Elsevier) pp 228–33
[59] Lucovhnikov A N and Novgorodov M Z 1971 *Short Rep. Phys. FIAN* **1** 27 (in Russian)
[60] Arslanbekov R R, Kudryavtsev A A and Khromov N A 1991 *Sov. J. Plasma Phys.* **17** 863 (in Russian)
[61] Fedorov V L 1985 *Sov. Phys.–Tech. Phys.* **30** 584
[62] Mezentsev A P, Mustafaev A S and Fedorov V L 1985 *Sov. Phys.–Tech. Phys.* **30** 332
[63] Fedorov V L and Mezentsev A P 1987 *Sov. Phys.–Tech. Phys.* **32** 363
[64] Kawano H, Annaratone V M and Allen J E 1991 *Proc. XX ICPIG (Pisa)* vol 5 (Pisa: CNR) p 1099
[65] Kazantsev S A and Subbotenko A V 1987 *J. Phys. D: Appl. Phys.* **20** 741
[66] Kazantsev S A and Subbotenko A V 1984 *Sov. Phys.–Tech. Phys. Lett.* **10** 1251
[67] Tochikubo F, Kokubo T, Kakuta S, Suzuki A and

Makabe T 1990 *J. Phys. D: Appl. Phys.* **23** 1184
[68] Vender D and Boswell R W 1990 *IEEE Trans. Plasma Sci.* **18** 725
[69] Wood V P, Lieberman M A and Lichtenberg A J 1991 *IEEE Int. Conf. on Plasma Sci. (Williamsburg, VA, June 1991)* report 5P13 (Piscataway, NJ: IEEE)
[70] Blagoev A B, Kagan Yu M, Kolokolov N B and Lyaguschenko R I 1974 *Sov. Phys.–Tech. Phys.* **19** 211, 215
[71] Karoulina E V and Levedev Yu A 1988 *J. Phys. D: Appl. Phys.* **21** 411
[72] Ferriera C M, Alves L L, Pinheiro M and Sa A B 1991 *IEEE Trans. Plasma Sci.* **19** 229
[73] Egorov V S 1980 *Spectroscopy of Gas Discharge Plasma* vol 2 (Leningrad: Leningrad State University) pp 53–80 (in Russian)
[74] Ivanov V A 1980 *Spectroscopy of Gas Discharge Plasmas* vol 2 (Leningrad: Leningrad State University) pp 81–121 (in Russian)
[75] Bletzinger P and Garscadden A 1991 *IEEE Int. Conf. on Plasma Sci. (Williamsburg, VA, June 1991)* report 3B1-2 (Piscataway, NJ: IEEE)
[76] Lawler J E and Den Hartog E A 1991 *Phys. Rev.* A **15** 4427
[77] Hebner G A, Verdeyen J T and Kushner M J 1988 *J. Appl. Phys.* **63** 2226